

CO₂-broadened water in the pure rotation and ν_2 fundamental regions

L.R. Brown^{a,*}, C.M. Humphrey^b, R.R. Gamache^b

^a *Jet Propulsion Laboratory, California Institute of Technology, Pasadena, CA 91109, USA*

^b *Department of Environmental, Earth & Atmospheric Sciences, University of Massachusetts Lowell, and University of Massachusetts School of Marine Sciences, 265 Riverside Street, Lowell, MA 01854-5045, USA*

Received 8 May 2007; in revised form 5 July 2007

Available online 23 August 2007

Abstract

The CO₂-broadened water coefficients (half-widths, line shifts, and temperature dependence of the widths) are predicted using a fully complex Robert–Bonamy formulation for the 937 allowed and forbidden perpendicular type transitions of (000)–(000) between 200 and 900 cm⁻¹ in order to facilitate atmospheric remote sensing of Mars and Venus. In addition, empirical Lorentz line widths and pressure-induced frequency-shifts of CO₂-broadened H₂¹⁶O are obtained at room temperature for 257 perpendicular transitions of the (010)–(000) fundamental. For this, calibrated spectra recorded at 0.0054 cm⁻¹ resolution are measured assuming Voigt line shapes. For transitions between 1287 and 1988 cm⁻¹ with rotational quanta up to $J = 13$ and $K_a = 6$, the widths vary from 0.045 to 0.212 cm⁻¹ atm⁻¹ at 300 K; the pressure-shifts are quite large and range from -0.0386 to $+0.0436$ cm⁻¹ atm⁻¹. For the (010)–(000) band, the RMS and mean observed and calculated differences for CO₂-broadened H₂O half-widths are 12% and -1.9% , respectively, while the RMS and mean ratios of the observed and calculated pressure-induced shift coefficients are 1.6 and 0.79, respectively. For pairs of transitions involving $K_a = 0$ and 1, such as $2_{02} \leftarrow 3_{13}$ and $3_{13} \leftarrow 2_{02}$, both the calculated and observed pressure induced shifts in positions are opposite in sign and often similar in magnitude. The data are too limited to characterize vibrational dependencies of the widths, however.

© 2007 Published by Elsevier Inc.

Keywords: Carbon dioxide broadened water; Theoretical calculations; Measurements; Half-widths; Pressure shifts; Vibrational dependence; Temperature dependence

1. Introduction

The present study uses new measurements of CO₂-broadening of water vapor within a single band at 6 μm (ν_2) in order to test theoretical models in both the rotational and fundamental regions. Such pressure broadening coefficients are required throughout the infrared for remote sensing of Mars and Venus. In both these planets, the most abundant species is carbon dioxide, but the two atmospheres are at very different pressures and temperatures. For Mars, the temperatures range from 150 to 300 K, and the pressures is only 10 mbars. For Venus, temperatures range from 200 to 750 K, but the pressure is very high (up to 90 bar at the surface). The present room temperature

measurements of the 6 μm fundamental provides the first comprehensive step towards satisfying these needs; presently there are numerous observations from ground-based and orbiting observatories (such as Venus Express [1] with the Venus IR Thermal Imaging Spectrometer [2] and the Mars Reconnaissance Orbiter Mission [3] with the Mars Climate Sounder [4]) being interpreted to understand the effects of water vapor on both of these planetary atmospheres [5–8]. The vibrational dependences of the broadening coefficients must be understood because the various instruments utilize water transitions at microwave, infrared and visible wavelengths.

A survey of the literature by Gamache et al. [9] for published measurements of CO₂-broadened water revealed that very few experimental widths [10–12] and no pressure-induced frequency shifts had been reported prior to 1994. The newer studies [13–17] increased the total number of

* Corresponding author. Fax: +1 818 354 5148.

E-mail address: Linda.R.Brown@jpl.nasa.gov (L.R. Brown).

measured widths to only 80, by reporting one perpendicular type transition in the rotational region [13] and four ν_2 lines at 1539 and 1652 cm^{-1} [14], and mostly parallel band transitions at 3963–4181 cm^{-1} [15], 7117–7186 cm^{-1} [16] and 7226–7233 cm^{-1} [17]; the pressure shifts were measured for 34 transitions [13,14,18].

The 257 empirical widths and shifts of (010)–(000) at 6 μm reported in this paper represent a substantial increase in the number of measured transitions, particularly for the pressure shifts. The measurements summarized in Table 1 are used to validate improved theoretical calculations, which are based on a complex implementation of the Robert–Bonamy theory [19]. There are no adjustable parameters in the formulation; nevertheless generally good agreement with measurements is obtained. To support planetary studies, the CO_2 -broadened H_2O coefficients in the far-IR are predicted for the allowed and forbidden rotational transitions (000)–(000) given in HITRAN 2004 [20]. We note that the validation is done for room temperature measurements of allowed perpendicular type transitions (i.e. $\Delta K_a = \pm 1$). Also, we do not investigate line shape effects such as line mixing [14] and Dicke narrowing [21], although both have been observed in water spectra.

2. Experimental details

The high resolution laboratory spectra for this study were recorded at 0.0054 cm^{-1} resolution with the Fourier transform spectrometer (FTS) located at the McMath Solar Telescope Facility on Kitt Peak in Arizona. The infrared radiation emitted from a global source was collected onto helium-cooled silicon single element detectors for the 1000–2700 cm^{-1} region. Each FTS run consisted of 12 or more interferograms co-added over a period of an hour to achieve a signal-to-noise ratio of 300:1 or better. A typical scan is shown in Fig. 1.

Dilute mixtures of water vapor and the foreign broadener, CO_2 , were made inside stainless steel absorption cells. A second cell in the optical beam contained low pressure CO in order to provide the calibration standard for line positions. The total sample pressures were measured to high accuracy (<0.5% uncertainty) using a 1000 torr head Baratron gauge whose calibration was verified by measuring the local atmospheric pressure (600 torr) with a Hg manometer. Temperatures of all the runs fell close to 300 K; these were monitored by thermistors in thermal contact with the exterior of the absorption cell. The experimental condi-

Table 1
Overview of present analysis for CO_2 -broadened water

	Experimental results	Calculated results
Number and range of transitions	ν_2 257 lines 1287–1988 cm^{-1}	Rotational transitions 937 lines 202–898 cm^{-1}
Min. and Max. J'	0 → 12	5 → 18
Min. and Max. K'_a	0 → 5	0 → 15
Widths in $\text{cm}^{-1} \text{atm}^{-1}$	0.0313 → 0.212	0.01 → 0.19
Shifts in $\text{cm}^{-1} \text{atm}^{-1}$	−0.0386 → 0.0436	−0.06 → 0.06

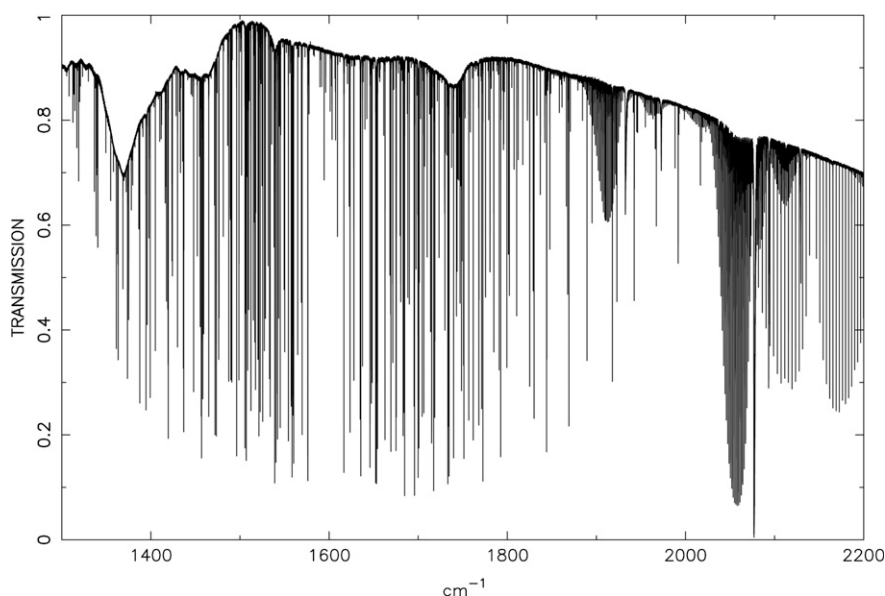


Fig. 1. The CO_2 -broadened spectrum of water in the ν_2 fundamental band recorded at 0.0054 cm^{-1} resolution with the McMath-Pierce Fourier transform spectrometer. The optical path is 1.5 m. The gas pressure of the mixture is 403 torr with the effective water pressure of 0.02 torr at 299.7 K. The features above 1890 cm^{-1} include bands of CO_2 ; a second cell containing low pressure CO was also used in order to provide calibration of the line positions.

Table 2
Experimental conditions^a

Run Number	Path (m)	Temp. (K)	Pressures (torr)	
			H ₂ O	CO ₂
1	1.50	300.3	0.40	242.0
2	1.50	300.3	0.21	300.0
3	1.50	300.4	0.08	347.0
4	1.50	300.2	0.25	397.0
5	1.50	299.7	0.02	403.0
6	1.50	300.3	1.18	451.0
7	1.50	299.6	0.36	596.0
8	1.50	300.0	2.00	764.0
9	1.50	299.6	1.84	991.0

Spectra were recorded at 0.0054 cm^{-1} resolution with a bandpass of $1000\text{--}2800\text{ cm}^{-1}$. For wavenumber (cm^{-1}) calibration, a 2nd cell was used simultaneously: path = 25 cm and pressure of CO ~ 0.05 torr

^a 760 torr = one atm = 101.3 kPa.

tions of the spectral runs are summarized in Table 2; all spectra were obtained with total sample pressures up to 993 torr for CO₂ + H₂O samples. Four of these spectra were used previously in a study of line mixing [14].

The empirical parameters were retrieved from the unapodized spectra using a nonlinear least-squares curve-fitting technique which adjusted the assumed values of positions, intensities and widths in the calculated spectrum to minimize the differences between the observed and synthetic spectra [22]. A sample retrieval is shown in Fig. 2 for two

ν_2 transitions: ($4_{23} \leftarrow 3_{30}$) near 1622.6 cm^{-1} and ($2_{11} \leftarrow 2_{02}$) near 1623.6 cm^{-1} . The observed and synthetic spectra are overlaid in the bottom panel, and their differences are displayed in the upper plot (% residual). The initial calculated positions, intensities and self-broadened widths were taken from previous work [23,24] with self-broadened widths held fixed. The initial H₂¹⁶O pressures were recorded before adding CO₂ to the sample, but during the data reduction, the H₂O partial pressures were checked by comparing retrieved line intensities to calculated line values [23]. Absorptions from residual water were reduced by evacuating the external path, the source enclosure and the FTS. Nevertheless, extra narrow features arose from a small amount of residual water (~ 0.02 torr) inside the FTS enclosure; these were effectively modeled by fitting each water line as two components, as seen in Fig. 2. In many cases, lines overlapped enough that several transitions had to be retrieved simultaneously. Badly blended features were generally not measured, particularly above 1900 cm^{-1} where CO₂ bands masked a number of the water transitions.

For each spectral feature, the CO₂-broadened H₂O half-width, line shift, position and relative intensity were obtained as averages based on three to nine spectra. In Table 3, an example is given for one transition by showing the individual retrievals from eight spectra and the averages. The columns have the pressure-shifted line position, line intensity with percentage uncertainty, half-width and

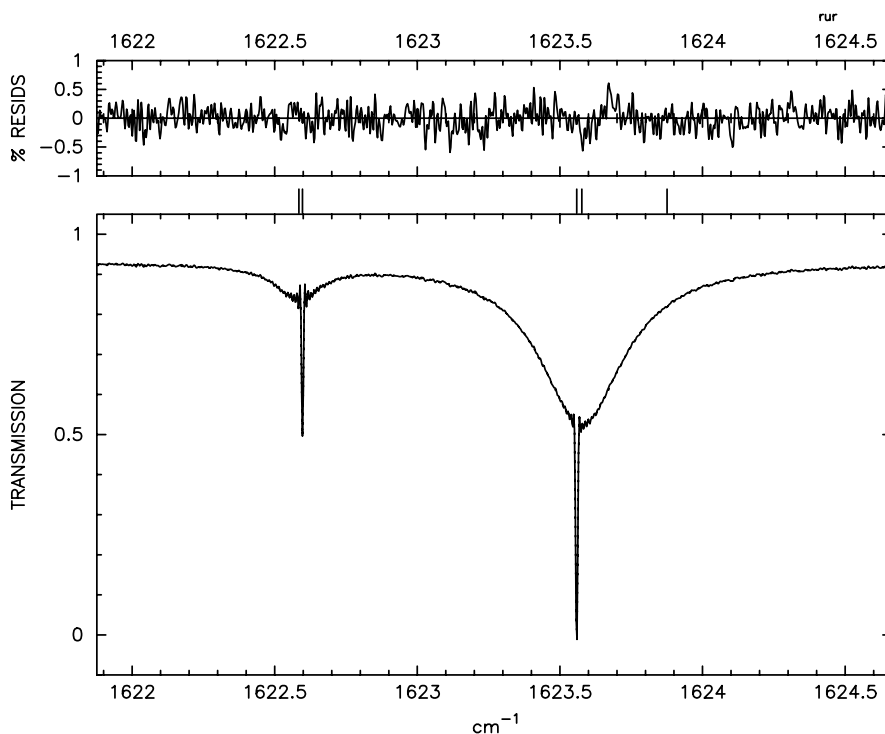


Fig. 2. Retrievals for pressure-broadened water lines near 1623 cm^{-1} . The narrow features arise from residual water vapor inside the FTS enclosure, while the wide features are from 0.36 torr of H₂O broadened by 596 torr of CO₂ at 299.6 K. The lower panel shows unapodized observed and synthetic spectra overlaid after line positions, intensities and widths have been adjusted by nonlinear least squares. The upper panel has the residual differences between the observed and calculated spectral digits. The pressure-induced frequency shifts are both positive (right line) and negative (left line).

Table 3
Individual measured values using H₂O + CO₂ mixtures^a

Observed position cm ⁻¹	Intens.	% unc	Width	% unc	Shift	Run Number
1501.83198	0.1572	-6.5	0.0903	-2.6	-0.01048	9
1501.83514	0.1748	4.0	0.0914	-1.4	-0.01045	8
1501.83767	0.1682	0.0	0.0939	1.3	-0.01016	7
1501.83949	0.1692	0.6	0.0935	0.9	-0.01036	6
1501.84004	0.1699	1.1	0.0938	1.2	-0.01071	4
1501.84149	0.1676	-0.3	0.0922	-0.5	-0.00910	3
1501.84187	0.1699	1.1	0.0905	-2.4	-0.00955	2
1501.84244	0.1712	1.8	0.0960	3.6	-0.01005	1
Average	0.1681	2.8	0.0927	2.0	-0.01011 (50)	

^a Positions are in cm⁻¹; intensities are in cm⁻² atm⁻¹ at 296 K; widths and shifts are in cm⁻¹ atm⁻¹ at 300 K.

its uncertainty and the pressure induced shift in the position; the last column has the run number of the spectrum used (see Table 2). The bottom row of the table has the averaged values of intensity, half-width and line shift. The shift is computed as the retrieved pressure-shifted position minus the calibrated zero pressure position [23], normalized to 1 atm pressure. The percentage uncertainties are computed as the difference between individual value and the average.

During the analysis, the pressure-induced frequency shifts were obtained two different ways. First, if a residual feature arising from water vapor inside the tank was sufficiently strong, the two retrieved line centers of the foreign-broadened and unbroadened residual water features were subtracted; for example in Fig. 2, for the right transition the shift is clearly positive, and the observed difference of 0.018 cm⁻¹ at 596 torr translates into a pressure shift of +0.023 cm⁻¹ atm⁻¹. In the second approach, a second cell of CO at low pressure in the beam permitted us to use the transitions of the 1–0 band of CO [25] as the calibration standard. The line shifts were then determined from the measured pressured shifted line positions of the broadened features minus the computed (zero pressure) positions [23] of the respective transitions. We also compared the CO calibration with one determined using residual water positions, and found that they agreed to within 0.00006 cm⁻¹. In principle, the self-broadened shifts (which are as large as 0.06 cm⁻¹/atm) can contribute to the total observed shift. For example, just as the observed half-width, γ , is related to the foreign and self-broadened coefficients, γ_f^o , and γ_s^o , respectively by,

$$\gamma = \gamma_f^o p_f + \gamma_s^o p_s, \quad (1)$$

where p_f and p_s are the foreign and self broadening pressures, respectively; a similar expression applies to the frequency-shifts:

$$\delta = \delta_f^o p_f + \delta_s^o p_s, \quad (2)$$

In fact, as seen in Table 2, the highest water pressure was only 2 torr, and very few shifts required adjustment to remove contributions from the self-broadened shift. In the end, all the shifts were obtained by the 2nd approach.

All the present measured CO₂-broadened H₂O coefficients of the ν_2 band are given in the (Appendix A) These were evaluated using experimental criteria, and values were omitted from consideration if (a) less than three spectra were used; (b) the observed line intensity was different from the calculated value by more than 15%; (c) the percentage uncertainties of the widths were greater than 10%. When a measured half-width was retained, the pressure shift was also kept even if the experimental uncertainty was greater than the observed shift (because sometimes the statistics are not reliable indicators of precision). Other studies [26,27] done with the Kitt Peak FTS produced half-widths that are clearly accurate to “3% or better,” and so it is thought that the present data have similar precisions for stronger transitions well isolated from other features; uncertainties for somewhat blended features can be worse. The best shifts for stronger well isolated transitions are thought to be determined with overall uncertainties of 0.0005 cm⁻¹. We note that line mixing may change the value of the apparent pressure shift. For example, four of the present spectra were measured previously with different

Table 4
Comparison with ν_2 CO₂-broadened H₂O retrieved with line mixing^a

J'	K_a	K_c	J''	K_a	K_c	Reference	H ₂ O + CO ₂ widths	Ratio of widths	Pressure shifts	Ratio of shifts
1	0	1	—	2	1	2	[14]	0.2001(1)	-0.0270	
2	1	2	—	1	0	1	[14]	0.2013	0.0262	
2	1	2	—	1	0	1	Present	0.1955	1.030	0.0267
2	1	2	—	3	0	3	[14]	0.1620	1.009	0.0099
2	1	2	—	3	0	3	Present	0.1605		0.0074
3	0	3	—	2	1	2	[14]	0.1627	1.032	-0.0098
3	0	3	—	2	1	2	Present	0.1577		-0.0089

The ratios are values of Brown et al. [14] divided by present values.

^a Widths and pressure shifts are in cm⁻¹ atm⁻¹ at 300 K.

retrieval software in order to investigate line mixing between two pairs of water transitions [14]; those retrieved broadening parameters are shown in Table 4 along with present values for three lines; the fourth line is removed because of its experimental uncertainties. The two sets of measurements agree within 3% or better for widths and 33% or better for shifts.

3. Theory

There have been a limited number of prior broadening calculations for water vapor transitions with CO₂ as the buffer gas. In 1971, Varanasi et al. [28] predicted widths of some ν_2 transitions by applying the theory of Anderson–Tsao–Curnutte (ATC) [29–32] using only the dipole–quadrupole interaction, straight line trajectories and the ATC cutoff procedure. It is now well accepted that such calculations have large uncertainty. In 1989, using approximations to the theory of Robert and Bonamy (RB) [19], Delay et al. [33] made new calculations in which they considered fictitious Q-branch transitions, no vibrational dependence, and the mean relative thermal velocity approximation. The half-widths for actual transitions were obtained from an algorithm derived by assuming nonresonance and that kinetic effects are negligible, providing estimates of the CO₂-broadened half-widths of water vapor. In 1995, Gamache et al. [15] calculated 562 transitions in the pure rotation band with $J'' = 0–12$ and $K''_a = 0–10$ using the real part of the Robert–Bonamy formulation. The assumed intermolecular potential was comprised of dipole–quadrupole and quadrupole–quadrupole terms and an atom–atom potential expanded to 4th order; trajectories were correct to second order in time, and the velocity integral was calculated. In the 1995 paper, the temperature dependence of the half-width was determined for 34 transitions. In 1997, Gamache et al. [18] applied the complex Robert–Bonamy calculations of the half-width and line shift for 31 transitions in the ν_1 , $2\nu_2$, and ν_3 bands of H₂O at 2.7 μm . The potential was that of the 1995 paper [15] with the addition of the isotropic induction and London dispersion potentials and the imaginary components of the electrostatic and atom–atom terms. It was found that the imaginary terms could change the value of the half-widths by as much as 25% and that the complex calculations gave much better agreement with measurement. Therefore, the present calculations reported in this study are based on the complex Robert–Bonamy (CRB) theory [19].

A full description of the formalism can be found in Refs. [34–36] so that only the salient features are presented here. The method is complex valued so that the half-width and line shift are obtained from a single calculation. By the use of linked-cluster techniques [37] the awkward cutoff procedure that characterized earlier theories [28–31] is eliminated. The dynamics are developed to second order in time giving curved trajectories based on the isotropic part of the intermolecular potential [19]. This has impor-

tant consequences in the description of close intermolecular collisions (small impact parameters). Also important for close collision systems is the incorporation in the RB theory of a short range (Lennard–Jones (6–12) [38]) atom–atom component to the intermolecular potential. This component has been shown to be essential for a proper description of pressure broadening, especially in systems where electrostatic interactions are weak [39,40] (here, the notion of strong and weak collisions adopts the definition of Oka [41]).

Within the CRB formalism the half width, γ , and line shift, δ , of a ro-vibrational transition $f \leftarrow i$ are given by minus the imaginary part and the real part, respectively, of the diagonal elements of the complex relaxation matrix. In computational form the half-width and line shift are usually expressed in terms of the scattering matrix [42,43]

$$(\gamma - i\delta)_{f \leftarrow i} = \frac{n_2}{2\pi c} \left\langle v \times \left[1 - e^{-R S_2(f, i, J_2, v, b)} e^{-i[S_1(f, i, J_2, v, b) + S_2(f, i, J_2, v, b)]} \right] \right\rangle_{v, b, J_2} \quad (3)$$

where n_2 is the number density of perturbers and $\langle \dots \rangle_{v, b, J_2}$ represents an average over all trajectories (impact parameter b and initial relative velocity v) and initial rotational state J_2 of the collision partner. S_1 (real) and $S_2 = {}^R S_2 + i {}^I S_2$ are the first and second order terms in the expansion of the scattering matrix; they depend on the ro-vibrational states involved and associated collision induced jumps from these levels, on the intermolecular potential and characteristics of the collision dynamics. The exact forms of the S_2 and S_1 terms are given in Refs. [34–36].

The S_1 term, which makes a purely imaginary contribution, is isotropic in the absence of any vibrational dependence of the anisotropic intermolecular forces. It then has the appellation of the vibrational dephasing term and arises only for transitions where there is a change in the vibrational state. The potential leading to S_1 is written in terms of the isotropic induction and London dispersion interactions:

$$V_{\text{iso}}^{\text{induction}} = -\frac{\mu_1^2 \alpha_2}{R^6}, \quad (4)$$

$$V_{\text{iso}}^{\text{dispersion}} = -\frac{3}{2} \frac{I_1 I_2}{I_1 + I_2} \frac{\alpha_1 \alpha_2}{R^6},$$

where μ_1 is the dipole moment of water vapor and α_k and I_k are the polarizability and ionization potential for water vapor ($k = 1$) and collision partner, CO₂, ($k = 2$). The vibrational dependence of these terms is contained in the dipole moment, μ_1 , and polarizability, α_1 , of water vapor. The first was investigated by Shostak and Muentner [44] and is given in Debyes by

$$\mu = 1.855 + 0.0051 \left(\nu_1 + \frac{1}{2} \right) - 0.0317 \left(\nu_2 + \frac{1}{2} \right) + 0.0225 \left(\nu_3 + \frac{1}{2} \right), \quad (5)$$

where v_n is the number of quanta in the n th normal mode. The polarizability of water vapor was obtained by Luo et al. [45] and is, in atomic units,

$$\alpha = 9.86 + 0.29 \left(v_1 + \frac{1}{2} \right) + 0.03 \left(v_2 + \frac{1}{2} \right) + 0.28 \left(v_3 + \frac{1}{2} \right). \quad (6)$$

The $S_2 = {}^R S_2 + i' S_2$ term is complex valued and results from the anisotropic interactions. The potential employed in the calculations consists of the leading electrostatic components for the H₂O–CO₂ pair (the dipole and quadrupole moments of H₂O with the quadrupole moment of CO₂) and atom–atom interactions [34,46]. The latter are defined as the sum of pair-wise Lennard–Jones (6–12) interactions [38] between atoms of the radiating (1) and the perturbing (2) molecules,

$$V^{\text{at-at}} = \sum_{i=1}^n \sum_{j=1}^m 4\epsilon_{ij} \left\{ \frac{\sigma_{ij}^{12}}{r_{1i,2j}^{12}} - \frac{\sigma_{ij}^6}{r_{1i,2j}^6} \right\}. \quad (7)$$

The subscripts $1i$ and $2j$ refer to the i th atom of molecule 1 and the j th atom of molecule 2, respectively, n and m are the number of atoms in molecules 1 and 2 respectively, and ϵ_{ij} and σ_{ij} are the Lennard–Jones parameters for the atomic pairs. The heteronuclear atom–atom parameters can be constructed from homonuclear atom–atom parameters (ϵ_i and σ_i) by the “combination rules” of Hirschfelder et al. [47] or Good and Hope [48]. The atom–atom distance, r_{ij} is expressed in terms of the center of mass separation, R , via the expansion in $1/R$ of Sack [49]. This development being truncated, sufficient order must be chosen to insure the convergence of calculated half-widths and line shifts, as has been discussed previously [34,35,46,50]. Here the formulation of Neshyba and Gamache [46] expanded to eighth order is used. Finally, recall that the isotropic component of the atom–atom potential is utilized to define the trajectory of the collisions within the semiclassical model of Robert and Bonamy [19].

For water vapor, the reduced matrix elements are evaluated using wavefunctions determined by diagonalizing the Watson Hamiltonian [51] in a symmetric top basis for the vibrational states involved in the transition. The Watson constants assumed were those of Matsushima et al. [52] for the ground state and from Flaud and Camy-Peyret [53] for the v_2 band. The rotational constant for CO₂ is $0.39021889 \text{ cm}^{-1}$ [54].

Many of the molecular parameters for the H₂O–CO₂ systems are well known and the present calculations use the best available values from the literature. The dipole and quadrupole moments of water vapor are taken from Refs. [44] and [55], respectively. There have been a number of measurements of the quadrupole moment of carbon dioxide [56] which range from 4.0 to roughly 4.6 in units of 10^{-26} esu. The most recent measurement [57] reports a value of $-4.02(10) \times 10^{-26}$ esu which is adopted in this work. The numerical values are listed in Table 5. The ionization potential of water is taken to be a vibrationally independent value of 12.6 eV [58]. For carbon dioxide the

Table 5
Values of the electrostatic moments of water vapor and CO₂

Molecule	Multipole (esu)	Reference
H ₂ O	$\mu = 1.8549(9) \times 10^{-18}$	[44]
	$\theta_{xx} = -0.13(3) \times 10^{-26}$	[55]
	$\theta_{yy} = -2.50(2) \times 10^{-26}$	[55]
	$\theta_{zz} = 2.63(2) \times 10^{-26}$	[55]
CO ₂	$\theta_{zz} = -4.02(10) \times 10^{-26}$	[57]

polarizability, $2.913 \times 10^{-24} \text{ cm}^3$, is taken from Ref. [59] and the ionization potential, 13.77 eV, from Ref. [60]. In the parabolic approximation, the isotropic part of the interaction potential is taken into account in determining distance, effective velocity, and force at closest approach [19]. To simplify the trajectory calculations, the isotropic part of the atom–atom expansion is fit to an isotropic Lennard–Jones (6–12) potential.

There are a number of different methods which have been proposed to determine heteronuclear potential parameters from homonuclear parameters [61,62, and references therein]. Good and Hope [48] showed that different combination rules used to determine ϵ cause variations of up to 15% in the final values. Thus the resulting parameters have an increased uncertainty (besides that resulting from the imprecision of the homonuclear data) which depends on the method chosen to go from the homonuclear to the heteronuclear parameters. From these facts, one can conclude that adjustment of the atom–atom parameters within $\sim 15\%$ around the values given by the combination formula of Hirschfelder et al. [47] is not unreasonable provided there are reliable experimental data on collisional parameters for adjustment. Here, the atom–atom parameters are determined by taking the homonuclear-atom–atom parameters from Bouanich [63], and using combination rules [47] to produce the heteronuclear atom–atom parameters. The values are presented in Table 6.

4. Broadening coefficients and discussion

In this section, the present observations and calculations of half-widths and pressure shifts for H₂O + CO₂ are examined and compared in order to understand their reliability for planetary applications. The predicted temperature dependence of the widths and the vibrational dependences of the parameters are discussed as well.

Table 6
Values of the heteronuclear atom–atom Lennard–Jones (6–12) parameters derived from homonuclear parameters

Atomic pair	$s/\text{\AA}$	e/k_B (K)
H–C	2.81	32.2
H–O	2.85	24.1
O–C	3.29	40.4
O–O	3.01	51.7

4.1. Half-widths and line shifts for “pairs” of transitions

It has been seen that the half-widths of some “pairs” of water transitions have similar values when a transition and its partner transition have the same upper and lower rotational state quantum numbers but reversed [24]. This is illustrated with calculated values in Table 7 and observed values in Table 8. In some cases, the pressure-induced shift coefficients are found to be opposite in sign and similar in magnitude.

This behavior is in fact predicted from theory. For a pure rotational transition (i.e. a transition within the same vibrational state) the S_1 term in the intermolecular potential vanishes so that the half-widths of the “pair” are identical and the line shifts are equal in magnitude and opposite in sign. This is seen in Table 7 using the calculations for the 183 GHz line of H_2O ($3_{13} \leftarrow 2_{20}$) broadened by CO_2 along with for the fictitious partner transition ($2_{20} \leftarrow 3_{13}$). For transitions that involve a change in vibrational quanta, such as (010)–(000), the vibrational dependence of the terms in Eq. (3) must be considered. The vibrational dependence of the half-width arises from two factors: one designated a spectroscopic effect and another that is purely a

vibrational effect. The first results from the fact that a change in the vibrational state leads to slightly different rotational wave functions, energy gaps, and transition probabilities between the rotational internal states. These changes affect the S_2 functions, but generally the effect is not great. The second factor is that a change of vibrational state in a transition leads to the S_1 term being non zero. For the half-width the general rule “half-widths for pairs are equal” should approximately hold as long as the S_1 term does not play a significant role (more on this below). The S_1 term is the dominant contribution to the line shift, which is given by a contribution from the final state minus the contribution from the initial state, $S_{1f} - S_{1i}$. Interchanging the initial and final state results in the line shift changing sign. As long as the vibrational dependence of other terms is small, the general rule “approximately equal in magnitude and opposite in sign” should hold. Thus for vibrational transitions where a small number of quanta are exchanged, these general rules should be valid. This is illustrated in Table 7 where CRB calculations of CO_2 -broadening of the H_2O transition ($3_{13} \leftarrow 2_{20}$) and the partner transition ($2_{20} \leftarrow 3_{13}$) in the ν_2 band are presented.

In Table 8 of measured values, the widths are arranged so that specific pairs of transitions can be listed together. In the top group, the first pair involves the same (J, K_a, K_c) rotational levels ($1_{01} \leftarrow 1_{10}$) and ($1_{10} \leftarrow 1_{01}$) which can also be labeled $^PQ_1(1)$ and $^RQ_0(1)$. For asymmetric rotors, the parameters K_m and J_m are defined as the maximum values of K_a and J , respectively, in the transition quanta. For example, as seen in the first and 2nd column of Table 8, the four lines in the top group are all $J_m = 1$ and $K_m = 1$ while those in the 2nd group are all $J_m = 4$ and $K_m = 2$. With this

Table 7
Calculated half-width and line shift for H_2O transition pairs^a

Rotation band	γ	δ
$3_{13} \leftarrow 2_{20}$	0.1677	-0.0238
$2_{20} \leftarrow 3_{13}$	0.1677	+0.0238
ν_2 band		
$3_{13} \leftarrow 2_{20}$	0.1659	-0.0243
$2_{20} \leftarrow 3_{13}$	0.1641	+0.0266

^a Widths (γ) and shifts (δ) are in $cm^{-1} atm^{-1}$ at 296 K.

Table 8
Examples of measured CO_2 -broadened H_2O coefficients^a

J_m	K_m	τ'	τ''	ΔK	ΔJ	J'	K'_a	K'_c	J''	K''_a	K''_c	ν	γ	% unc	% obs.–cal.	δ	(unc)	obs./cal.
1	1	0	0	p	Q	1	0	1	1	1	0	1576.185	0.2101	2.2	1.0	-0.0262	(8)	0.985
1	1	0	0	r	Q	1	1	0	1	0	1	1616.711	0.2122	2.1	1.3	0.0240	(37)	1.109
1	1	0	1	p	P	0	0	0	1	1	1	1557.609	0.1921	2.2	-7.3	-0.0293	(12)	0.984
1	1	1	0	r	R	1	1	1	0	0	0	1634.967	0.2008	0.7	-3.7	0.0332	(4)	0.836
4	2	0	0	p	Q	4	1	3	4	2	2	1559.690	0.1766	0.9	-2.6	-0.0281	(7)	0.735
4	2	0	0	r	Q	4	2	2	4	1	3	1647.404	0.1682	1.0	-7.7	0.0303	(6)	0.767
4	2	1	0	p	R	3	1	3	4	2	2	1423.704	0.1616	0.9	-4.9	-0.0230	(9)	0.973
4	2	0	1	r	P	4	2	2	3	1	3	1780.623	0.1571	2.0	-6.2	0.0287	(59)	1.009
4	2	1	1	p	Q	4	1	4	4	2	3	1521.235	0.1202	2.1	-2.0	-0.0072	(26)	1.989
4	2	1	1	r	Q	4	2	3	4	1	4	1683.178	0.1141	1.8	-6.1	0.0132	(3)	1.076
6	5	0	0	r	Q	6	5	1	6	4	2	1795.100	0.0953	3.6	-9.1	-0.0053	(33)	2.190
6	5	0	0	p	Q	6	4	2	6	5	1	1510.533	0.0901	3.1	-10.8	0.0016	(24)	1.705
6	5	0	1	r	R	6	5	1	5	4	2	1942.765	0.0953	4.5	5.0	-0.0074	(15)	1.293
6	5	1	0	r	R	6	5	2	5	4	1	1942.516	0.0953	1.6	0.1	-0.0096	(4)	1.388
6	5	1	1	r	Q	6	5	2	6	4	3	1796.133	0.0973	1.9	0.6	-0.0031	(22)	2.464
8	1	1	0	r	R	8	1	8	7	0	7	1751.423	0.0822	1.7	27.7	0.0074	(3)	2.395
8	2	1	0	r	R	8	2	7	7	1	6	1790.952	0.0999	1.8	-12.8	0.0203	(3)	1.371
8	3	1	0	r	R	8	3	6	7	2	5	1847.783	0.1136	1.9	-14.0	0.0270	(16)	0.812
8	4	1	0	r	R	8	4	5	7	3	4	1922.341	0.1190	1.1	-11.3	-0.0188	(65)	1.156
8	5	1	0	r	R	8	5	4	7	4	3	1988.396	0.1007	3.0	-9.6	-0.0154	(26)	1.628

^a Measured positions (ν) are in cm^{-1} ; widths (γ) and shifts (δ) are in $cm^{-1} atm^{-1}$ at 300 K. The value of τ is $K_a + K_c - J$. Transitions can be grouped into four “family” subsets according to the value of $\Delta\tau = \tau' - \tau''$: (i) 0–0 (ii) 1–1 (iii) 0–1 and (iv) 1–0. The Q branch lines have $\Delta\tau = 0$ (i.e. subgroups i and ii) and P and R branches have $\Delta\tau = 1$ or -1 (i.e. subgroups iii and iv).

grouping, it becomes apparent that the widths of certain pairs are nearly equal, similar to the situation seen in diatomic molecules [65] where the widths of $P(J'')$ is similar to the width of $R(J'' + 1)$: $P1 = R0$, $P2 = R1$, etc. For water broadened by carbon dioxide, the pressure shifts of the pairs are often opposite in sign and sometimes similar in magnitude, as discussed above.

The half-width and line shift from the CRB theory depend on both the real and imaginary components of the intermolecular potential, an effect not seen in ATC theory [29–32]. The S_1 term, which depends on the vibrational dependence of the polarizability and dipole moment, is proportional to the number of vibrational quanta exchanged in the transition (see Eqs. (4–6)). For transitions involving large changes in the vibrational state, the magnitude of the line shift should increase and, for H_2O , become more negative. Thus, as the number of vibrational quanta transferred in a transition increases, one should expect the general rules discussed above to be less valid. In addition Gamache and Hartmann [64] have shown that certain types of transitions of water vapor in a bath of N_2 , O_2 , or air have an unusually large dependence on vibration. The results of this study indicate that CO_2 -broadening of water vapor has similar behavior, and the general rules will be less valid for transitions with $K_c = J$.

Another factor that enters into the general rule for the line shift is that the calculation of each component, initial and final state, has negative and positive contributions which sum to the final value. Cancellation occurs with the difference between two large numbers usually being the final line shift. Thus, for small line shifts we do not expect the rule to work well, for line shifts large in magnitude the rule should be more reasonable.

4.2. Half-widths and line shifts for “families” of transitions

At first glance, the measurements may appear to have no obvious relationship to the quantum numbers, but some patterns can be discerned if the broadening coefficients are organized into specific groups. Another pattern is seen by sorting the six widths in descending order for the 2nd group ($J_m = 4$, $K_m = 2$). Transitions can be separated into subsets [24,66] according to the value of $\tau = K_a + K_c - J$ in both the upper and lower states, as shown in the 3rd and 4th columns of Table 8. In the last group in Table 8, lines of $J_m = 8$ with $\tau' = 1$ and $\tau'' = 0$ are listed for ascending values of $K_m (=1 \rightarrow 5)$ to show that for this “family” the widths increase slightly with increasing K_m .

The patterns are further illustrated in Fig. 3 which shows the measured CO_2 -broadened H_2O widths of (010)–(000) versus J_m for $K_m = 2$. Inspection reveals that for $K_m = 2$, the transitions involving $\tau' = \tau'' = 0$ have the largest widths at low J_m while the ones with $\tau' = \tau'' = 1$ have the smallest values; the intermediate values occur for $\tau' \neq \tau''$. In contrast, the widths for the $J_m > 6$, the widths are nearly the same.

These observations provide additional evaluation of the experimental precisions. In Table 8, the percentage uncertainty of the measured width and the percentage difference between the observed and theoretically calculated values are shown in columns 14 and 15, respectively. Clearly, one has more confidence in measurements if the widths of pairs (by J_m , K_m , τ , ΔK_a , ΔJ) are nearly the same or if values change smoothly as a function of J_m or K_m . In Table 8, the shift uncertainty in the last two digits and the ratio of the observed and calculated shifts are also listed, and one must conclude that experimental uncertainties of the shifts alone are less reliable indications of those precisions.

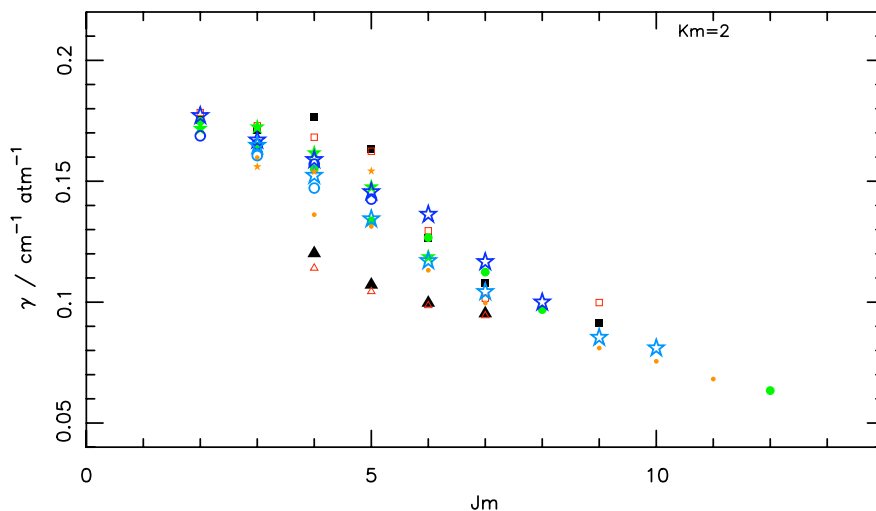


Fig. 3. The observed widths of H_2O broadened by CO_2 (in $cm^{-1} atm^{-1}$ at 300 K) versus J_m . The values plotted are for (010)–(000) transitions with $K_m = 2$ where J_m and K_m are, respectively, the maximum values of J and K_a of transitions and $\tau = K_a + K_c - J$ (see Table 8). The four “families” according to τ', τ'' are distinguished by (\square) for $\tau' = \tau'' = 0$; (\triangle) for $\tau' = 1, \tau'' = 1$; ($*$) for $\tau' = 0, \tau'' = 1$; and (\circ) for $\tau' = 1, \tau'' = 0$. Open symbols are used for ΔK_a equal +1 and solid symbols for ΔK_a equal -1 . At lower J_m , the Q branch transitions with $\tau' = \tau'' = 1$ have smaller widths while the Q branch transitions with $\tau' = \tau'' = 0$ tend to be larger.

4.3. The far-IR rotational transitions from 200 to 900 cm^{-1}

Water transitions from 200 to 900 cm^{-1} were considered explicitly in order to provide broadening parameters for remote sensing by the Mars Reconnaissance Orbiter [3,4]. Complex Robert–Bonamy calculations were made for CO_2 -broadening of 937 water vapor transitions from HITRAN [20] for the rotational band of the principal isotopologue with $J_{\text{max}} \leq 18$. The calculations employed the velocity integral form of the CRB equations (see Eq. (3)). A representative sample of the prediction is shown in Table 9. The transitions are Q and R branch lines, and many are forbidden with $\Delta K_a = 3, 5, 7$.

In Fig. 4a and b, the calculated CO_2 -broadened water widths and pressure-induced frequency shifts (in $\text{cm}^{-1} \text{atm}^{-1}$ at 296 K) are plotted, respectively, as a function of $K_m + 0.1 (J_m - K_m)$ where J_m and K_m are

described above. The plot symbol is the value of J_m , and the values of $|\Delta\tau|$ are distinguished by the font size. Recall that in perpendicular bands of water, the ${}^r\text{Q}$ and ${}^p\text{Q}$ type transitions have $\Delta\tau = 0$ [66], thus permitting those transitions to be recognized easily in the plot. The offset term of 0.1 ($J_m - K_m$) is used to separate values in order to reveal the variation of the coefficients by J_m within a K_m group. The calculated widths range from 0.01 to 0.19 $\text{cm}^{-1} \text{atm}^{-1}$. At low K_m , the widths decrease sharply with increasing J_m , while at higher K_m , some widths increase with increasing J_m ; some groups both fall and then rise with increasing J_m . At higher K_m , the patterns for $|\Delta\tau| = 0$ (Q branch lines) are different from those of $|\Delta\tau| = 1$ (the P and R branch transitions).

In contrast, patterns are more difficult to discern for the pressure shifts shown in Fig. 4b. The calculated shifts of the rotational transitions in this region are both negative and positive. They vary between -0.06 and $0.06 \text{cm}^{-1} \text{atm}^{-1}$, and the mean shift is $0.003 \text{cm}^{-1} \text{atm}^{-1}$.

Table 9

Sample of calculated CO_2 -broadened H_2O parameters of (000)–(000)^a

$J'_{K_a K_c}$	$J''_{K_a K_c}$	γ	δ
4 ₄₀	3 ₃₁	0.1058	–0.0067
4 ₄₁	3 ₃₀	0.1103	–0.0115
5 ₅₀	4 ₄₁	0.0873	–0.0049
5 ₄₁	4 ₃₂	0.0998	–0.0059
5 ₄₂	4 ₃₁	0.1186	–0.0170
5 ₃₂	4 ₂₃	0.1352	0.0239
5 ₂₃	4 ₁₄	0.1599	0.0201
6 ₅₁	5 ₄₂	0.0860	–0.0095
6 ₄₂	5 ₃₃	0.0996	0.0045
6 ₃₃	5 ₂₄	0.1406	0.0284
6 ₅₂	5 ₄₁	0.0908	–0.0131
6 ₄₃	5 ₃₂	0.1273	–0.0187
6 ₃₄	5 ₂₃	0.1508	–0.0104
7 ₇₀	6 ₂₅	0.1321	0.0076
7 ₅₂	6 ₄₃	0.0854	–0.0109
7 ₃₄	6 ₂₅	0.1378	0.0280
7 ₃₅	6 ₂₄	0.1295	0.0049
7 ₂₅	6 ₁₆	0.1304	–0.0123
7 ₅₃	6 ₄₂	0.0952	–0.0179
8 ₇₁	8 ₀₈	0.1322	0.0051
8 ₄₄	7 ₃₅	0.1186	0.0255
9 ₉₀	9 ₄₅	0.1289	–0.0181
10 ₉₁	9 ₆₄	0.0942	0.0024
10 ₉₁	10 ₄₆	0.1224	–0.0179
10 ₁₉	9 ₂₈	0.0535	0.0015
10 ₉₂	9 ₆₃	0.0946	0.0025
10 ₇₄	9 ₂₇	0.1181	0.0266
10 ₃₈	9 ₂₇	0.1203	0.0305
10 ₂₉	9 ₁₈	0.0605	0.0276
11 ₀₁₁	10 ₁₁₀	0.0387	0.0097
11 ₉₂	11 ₄₇	0.1117	–0.0099
11 ₂₉	10 ₃₈	0.0658	–0.0391
11 ₁₁₀	10 ₂₉	0.0469	0.0069
11 ₉₃	10 ₆₄	0.0867	–0.0050
11 ₁₁₁	10 ₀₁₀	0.0386	0.0096
12 ₁₁₂	11 ₀₁₁	0.0353	0.0104
13 ₀₁₃	12 ₁₁₂	0.0317	0.0071
13 ₅₈	12 ₂₁₁	0.1129	0.0241
14 ₇₇	13 ₄₁₀	0.0788	0.0395
16 ₃₁₄	15 ₀₁₅	0.0605	–0.0044
17 ₃₁₄	16 ₂₁₅	0.0559	–0.0059

^a The widths (γ) and shifts (δ) are in $\text{cm}^{-1} \text{atm}^{-1}$ at 296 K.

4.4. The ν_2 fundamental (010)–(000) at 6 μm

The measured and corresponding calculated CO_2 -broadened half-width and pressure-induced frequency-shift coefficients are presented in the (Appendix A) for 257 transitions of the ν_2 fundamental. The columns are the rotational quantum numbers (J , K_a , K_c), the line position, the measured half-width in $\text{cm}^{-1} \text{atm}^{-1}$ at 300 K with the experimental uncertainty, and the calculated value with the percentage difference between the observed and calculated values. Also listed are the observed pressure shifts in $\text{cm}^{-1} \text{atm}^{-1}$ at 300 K with the uncertainty in the last digits, the calculated shift and the ratio between observed and calculated shifts, as well as the computed temperature coefficient and its maximum calculated error (described later). The line position is the zero pressure line position computed from term values [20,23]; with one exception, all the rotational quantum assignments are the stronger allowed transitions of the ν_2 band.

In Fig. 5, the ν_2 half-widths are plotted versus $K_m + 0.1 (J_m - K_m)$. The factor added to K_m is to spread the points out according to the oblate–prolate limit of the states, and the symbols used in Fig. 4 are applied in this figure as well. The use of an enlarged font for $|\Delta\tau| = 0$ permits Q branch lines to be discerned. In the upper panel, the observed half-widths in $\text{cm}^{-1} \text{atm}^{-1}$ at 300 K vary by almost a factor of five from 0.045 (for $J_m = 13$, $K_m = 1$) to 0.212 (for $J_m = 1$, $K_m = 1$). In the lower panel, the observed–calculated differences in percent are shown; the majority of the residuals fall between $\pm 10\%$ with larger systematic deviations up to 40% for higher J_m lines of $K_m = 1$ and 2.

Similarly, the observed ν_2 shifts and the ratios of observed to calculated shifts are shown in the upper and lower panels of Fig. 6, respectively. The observed pressure-shifts range from -0.0386 (for $J_m = 7$, $K_m = 3$, $\tau' = \tau'' = 0$) to $+0.0436 \text{cm}^{-1} \text{atm}^{-1}$ (for $J_m = 8$, $K_m = 3$, $\tau' = \tau'' = 0$). The RMS and mean observed and calculated

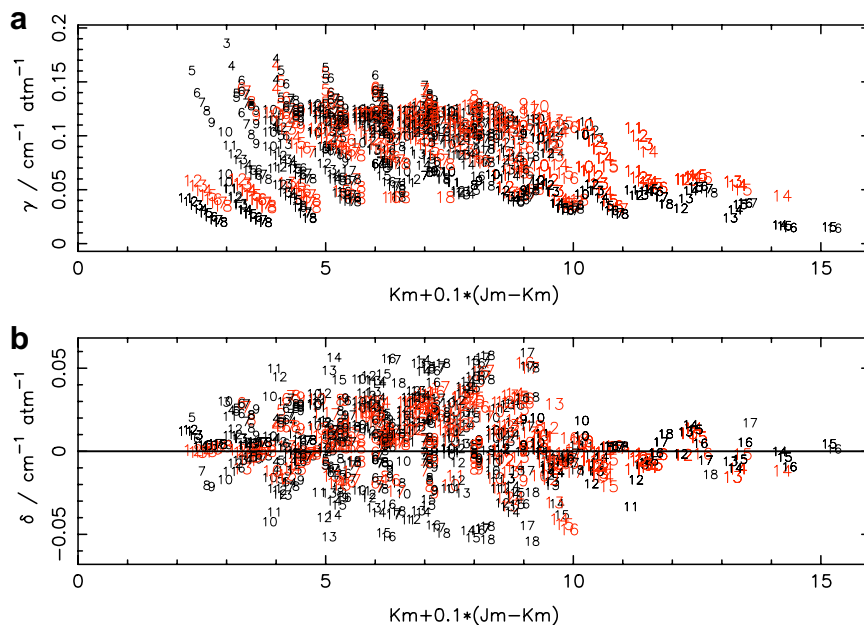


Fig. 4. The calculated CO_2 -broadened coefficients of H_2O for the (000)–(000) transitions between 200 and 900 cm^{-1} . The upper trace (a) has widths and the lower trace (b) the pressure-induced frequency shifts in $\text{cm}^{-1}\text{ atm}^{-1}$ at 296 K. Values are plotted as a function of $K_m + 0.1(J_m - K_m)$, and the plot symbol is J_m . J_m and K_m are, respectively, the maximum values of J and K_a in the transition. $\tau = K_a + K_c - J = 0$ or 1, and $\Delta\tau = \tau' - \tau''$. The larger symbols are Q branch lines with $\Delta\tau = \tau' - \tau'' = 0$, and the smaller ones are P and R branch transitions with $\Delta\tau = \tau' - \tau'' \neq 0$.

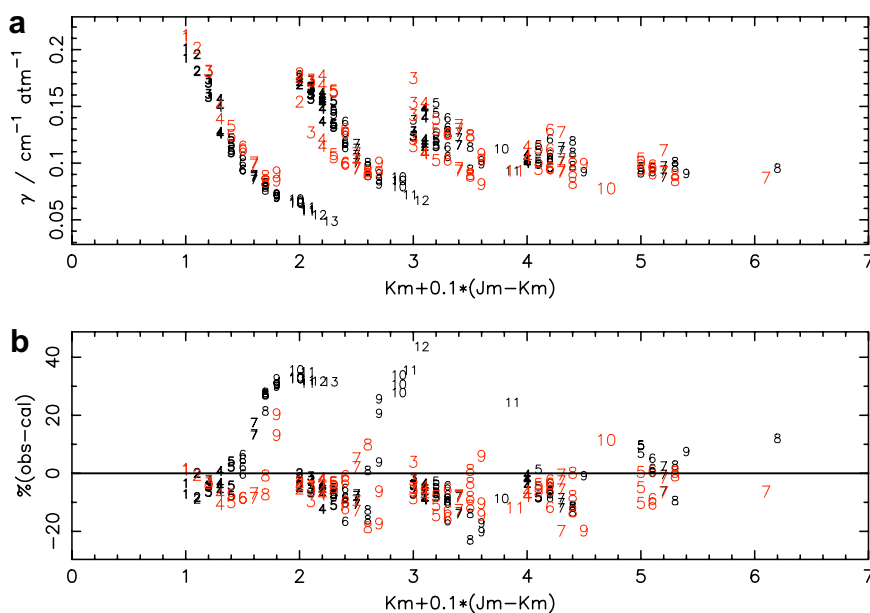


Fig. 5. The observed widths of H_2O broadened by CO_2 in $\text{cm}^{-1}\text{ atm}^{-1}$ at 300 K for allowed (010)–(000) transitions between 1280 and 1988 cm^{-1} versus $K_m + 0.1(J_m - K_m)$. The upper trace (a) has widths and the lower trace (b) the pressure-induced frequency shifts in $\text{cm}^{-1}\text{ atm}^{-1}$ near 300 K. The plot symbol is J_m . J_m and K_m are, respectively, the maximum values of J and K_a in the transition. $\tau = K_a + K_c - J = 0$ or 1, and $\Delta\tau = \tau' - \tau''$. The larger symbols are Q branch lines with $\Delta\tau = \tau' - \tau'' = 0$, and the smaller ones are P and R branch transitions with $\Delta\tau = \tau' - \tau'' \neq 0$.

differences for CO_2 -broadened H_2O half-widths are 12% and -1.9% , respectively, while the RMS and mean ratios of the observed and calculated pressure-induced shift coefficients are 0.79 and 1.6, respectively, if a few suspicious measurements are not considered.

4.5. Temperature dependence of the half-width

For planetary studies, the temperature dependence of the half-widths must be known. Theoretical consideration of the temperature dependence of the half-width for a

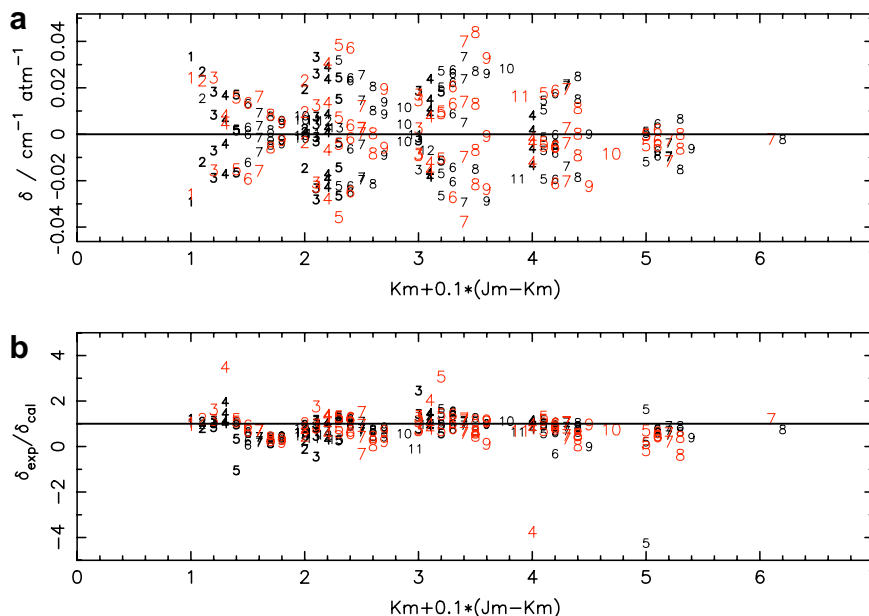


Fig. 6. The observed pressure shifts of H₂O broadened by CO₂ in cm⁻¹ atm⁻¹ near 300 K for allowed (010)–(000) transitions between 1280 and 1988 cm⁻¹ versus $K_m + 0.1 (J_m - K_m)$. The measured values and the ratios of observed to calculated shifts are shown, respectively, in the upper (a) and lower (b) traces. The plot symbol is J_m . J_m and K_m are, respectively, the maximum values of J and K_a in the transition. $\tau = K_a + K_c - J = 0$ or 1, and $\Delta\tau = \tau' - \tau''$. The larger symbols are Q branch lines with $\Delta\tau = \tau' - \tau'' = 0$, and the smaller ones are P and R branch transitions with $\Delta\tau = \tau' - \tau'' \neq 0$.

one term intermolecular potential gives the power law model,

$$\gamma(T) = \gamma(T_0) \left[\frac{T_0}{T} \right]^n. \quad (8)$$

However, for certain types of radiator–perturber interactions the power law model is being questioned. Wagner et al. [67] have observed that for certain transitions of water vapor perturbed by air, N₂ or O₂ the power law does not correctly model the temperature dependence of the half-width. This fact was also demonstrated by Toth et al. [68] in a study of air-broadening of water vapor transitions in the region from 696 to 2163 cm⁻¹. In both studies it was found that the temperature exponent, n , can be negative for many transitions. In such cases the power law Eq. (8) is not valid. The mechanism leading to negative temperature exponents is called the resonance overtaking effect and was discussed by Wagner et al. [67], Antony et al. [69] and Hartmann et al. [70]. Antony et al. showed that for self-broadening of water vapor that there are always enough collisions that are on resonance where the resonance overtaking effect can be neglected.

The importance of the resonance overtaking effect was investigated here for the H₂O + CO₂ system. The widths were calculated at eight different temperatures (200, 225, 275, 296, 350, 400, 450, and 500 K) for the 937 transitions in the rotation region and fitted to Eq. (8); the resulting temperature exponents n ranged from -0.23 to 0.91 . For example, $\ln[\gamma(T)/\gamma(T_0)]$ versus $\ln[T_0/T]$ values are plotted in Fig. 7. As seen in the upper panel for the $6_{34} \leftarrow 5_{23}$ transition, the correlation coefficient of the fit is 0.999, i.e. the model is near perfect. In contrast, in the lower panel of

Fig. 7, a negative value of n was obtained for the $16_{152} \leftarrow 15_{141}$ transition with a correlation coefficient of -0.898 , indicating a very poor fit to Eq. (8). These simulations suggest that the power law in Eq. (8) is a reasonable model temperature for some transitions (perhaps lower values of J and K_a) but fails for others (higher J and K_a). However, it appears that the power law model can give reasonable estimates for the H₂O–CO₂ system over short temperature ranges.

Because the application here is to interpret the atmosphere of Mars, the temperature exponents in the (Appendix A) were recalculated using the temperature data at 200, 225, 275, and 296 K, giving more reliable values of n from the power law model. For Venus studies, perhaps a better model would be an interpolation scheme using the eight temperatures of this study. We note that there are no measurements for the temperature dependence of the half-widths or the pressure shifts.

The calculated temperature exponents of the rotational and v_2 transitions are plotted versus $J_m + 0.1 (J_m - K_m)$ in Fig. 8, where the larger size symbols are used for v_2 . Birnbaum [71] has shown that for a system that has only the “dipole–quadrupole” interaction, the temperature exponent is 0.83. This is the leading interaction of the H₂O–CO₂ system. The temperature exponents in Fig. 8 range from ~ 1.01 to -0.15 showing a large variation from the value for a pure “dipole–quadrupole” system and from the average temperature exponent of 0.71. Finally the error in the temperature exponent was determined as follows. The temperature exponents were calculated using the half-width values at any two of the temperatures studied. With four temperatures this yields six 2-point temperature

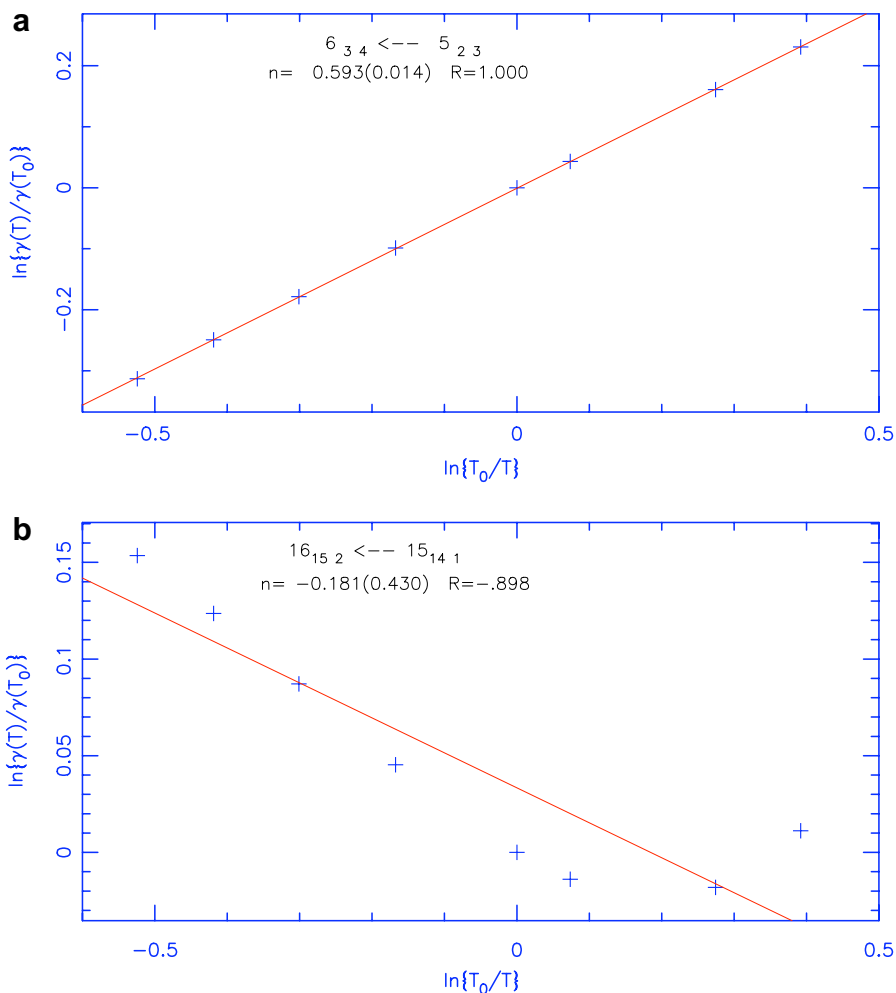


Fig. 7. The effective temperature dependence coefficient n in Eq. (8) determined by fitting calculated widths at different temperatures. The n values for a lower J , K_a transition can be modeled to a straight line as a function of $\ln\{T_0/T\}$ as seen in the upper trace (a), but not for a high J , high K_a transition shown in the lower trace (b). R is the correlation coefficient; the value in parentheses is the uncertainty. The temperatures are 200, 225, 275, 296, 375, 400, 450, and 500 K.

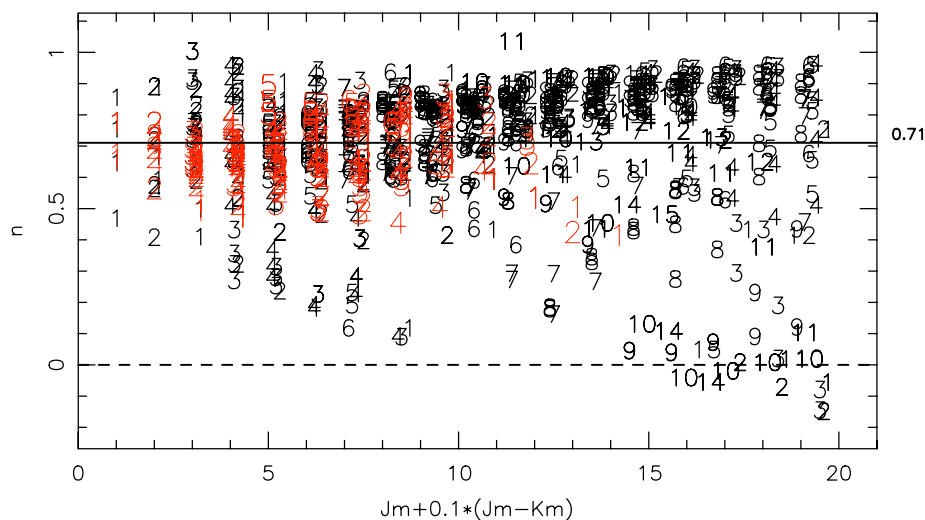


Fig. 8. The calculated temperature dependence coefficients n of the widths versus $J_m + 0.1(J_m - K_m)$ for both (000)–(000) and (010)–(000) transitions considered in this study. The plot symbol is the value of K_m . The values for (000)–(000) are both allowed and forbidden transitions while those of (010)–(000) are all allowed, with one exception. Symbols for (000)–(000) are smaller in size than the ones for (010)–(000).

exponents. The difference between each 2-point temperature exponent and the 4-point fit value is calculated. The error is taken as the largest of these differences. While this procedure tends to yield the maximum error in the temperature exponent, given the nature of the data and other uncertainties it is thought to be more reasonable than a statistical value taken from the fit.

4.6. Comparison of (000)–(000) and (010)–(000) broadening coefficients

The calculations presented above for 937 transitions of the rotation band of H₂O perturbed by CO₂ show that half-widths change by almost a factor of 20. This fact suggests that vibrational dependence may be important, especially for transitions involving levels with $K_c = J$. In the present study, there are 31 ν_2 transitions in common in the rotational calculations that can be used to investigate possible vibrational dependence of the allowed lines. In Fig. 9a the percent difference between the calculated half-width in the rotation band minus that in the ν_2 band are plotted versus $J_m + 0.1(J_m - K_m)$. While it is expected that the vibrational dependence of the half-width will be smallest for comparison of the rotation to the ν_2 band (see Ref. [64,72] for details), the figure clearly shows some dependence on the vibrational state in that the widths of the higher K_a lines deviate more than the low K_a lines. The average percent difference is small, -0.81 , however, the average absolute difference is 3.6% with some values reaching 10%. As seen in Fig. 9b, which shows the ratio of the shifts for the two bands, the shifts can be different by a factor of 2; the average ratio is 0.95. Thus, while the number of comparisons is small, it can be concluded that these

broadening coefficients for H₂O transitions perturbed by CO₂ are not the same in both bands.

4.7. The vibrational dependence of broadening coefficients

Water transitions with the same rotational quantum numbers but in different bands have different broadening parameters. This was predicted from the CRB theory by Gamache and Hartmann [64] who suggested that the half-width and line shift approximately follow the formulas

$$\begin{aligned} \gamma[(v'_1, v'_2, v'_3)f \leftarrow (v''_1, v''_2, v''_3)i] \\ = \gamma_{f-i}^0 + A_{f-i} \times (0.3\Delta v_1 + 0.07\Delta v_2 + 0.3\Delta v_3)^2, \\ \delta[(v'_1, v'_2, v'_3)f \leftarrow (v''_1, v''_2, v''_3)i] \\ = \delta_{f-i}^0 + B_{f-i} \times (0.3\Delta v_1 + 0.07\Delta v_2 + 0.3\Delta v_3). \end{aligned} \quad (9)$$

The air broadening measurements reported by the Brussels-Reims groups [73,74] up to 25000 cm⁻¹ revealed that there is a large vibrational dependence of the half-width for certain H₂O transitions. Later, Jacquemart et al. [75] obtained the coefficients in these formulas for air-broadening by fitting a massive collection of air-broadening measurements from the microwave to the visible (such as [73,74,76,77]).

Measurement to measurement comparisons were attempted for other water bands, as shown in Table 10. Unfortunately, the present CO₂-broadened water measurements of strong, allowed, perpendicular transitions in ν_2 were in common with only one rotational transition from Golubiatnikov et al. [13], four transitions of Gamache et al. at 2.5 μm [15], three transitions of Nagali et al. at 1.4 μm [16] and the three lines of Langlois et al. at

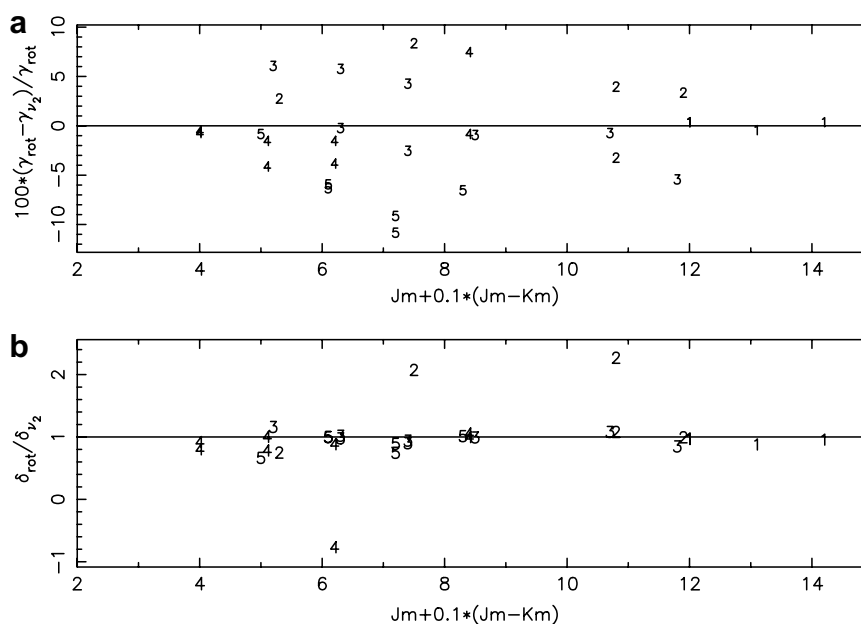


Fig. 9. Comparison of observed (010)–(000) and calculated (000)–(000) broadening coefficients. The plot symbol is K_m . The upper panel (a) has the percentage difference of widths versus $J_m + 0.1(J_m - K_m)$ for transitions with the same rotational quantum numbers. In the bottom panel (b), the ratio is the observed (010)–(000) shift to calculated (000)–(000) shift for H₂O broadened by CO₂.

Table 10
Comparison of measured CO₂-broadened H₂O widths^a

J'	K_a	K_c	J''	K_a	K_c	Band	Reference	γ	% unc	Ratio $\gamma^{v_{\text{vib}}}/\gamma_{v_2}$	
3	1	3	—	2	2	0	gs	[13]	0.157		1.006
3	1	3	—	2	2	0	v_2	Present	0.1560	(2.7)	
2	2	0	—	3	1	3	v_2	Present	0.1603	(4.7)	
9	5	4	—	8	4	5	v_1	[15]	0.085	(4.7)	0.94
8	4	5	—	9	5	4	v_2	Present	0.0903	(1.1)	
3	2	1	—	3	1	2	$2v_1$	[17]	0.187	(9.6)	1.07
3	2	1	—	3	1	2	v_2	Present	0.173	(1.7)	
3	1	2	—	3	2	1	v_2	Present	0.171	(2.9)	
4	2	2	—	4	1	3	$2v_1$	[17]	0.172	(25.)	0.99
4	2	2	—	4	1	3	v_2	Present	0.170	(2.9)	
4	1	3	—	4	2	2	v_2	Present	0.178	(2.4)	
5	2	3	—	5	1	4	$2v_1$	[17]	0.196	(3.5)	1.21
5	2	3	—	5	1	4	v_2	Present	0.1624	(1.2)	
5	1	4	—	5	2	3	v_2	Present	0.1634	(2.0)	
4	1	4	—	4	2	3	$2v_1$	[16]	0.109	(22.0)	0.93
4	1	4	—	4	2	3	v_2	Present	0.120	(2.1)	
4	2	3	—	4	1	4	v_2	Present	0.1141	(1.8)	
4	3	2	—	5	2	3	$2v_1$	[16]	0.138	(5.0)	1.14
4	2	3	—	5	3	2	v_2	Present	0.1257	(1.0)	
5	3	2	—	4	2	3	v_2	Present	0.1162	(1.5)	
4	2	2	—	4	3	1	$2v_1$	[16]	0.140	(16.)	0.92
4	3	1	—	4	2	2	v_2	Present	0.152	(1.9)	

^a The linewidths (HWHM) are in units of $\text{cm}^{-1} \text{atm}^{-1}$ at 300 K. The other measurements are from: Golubiatnikov et al. [13]; Gamache et al. [15]; Langolis et al. [17] and Nagali et al. [16].

1.3 μm [17]. The number is very limited because one study reported weak transitions in the wings of bands [15,18] while the other two investigations measured small spectral intervals with diode laser spectrometers [16,17]. Thus, no conclusion could be reached about vibrational dependence using experimental data of CO₂-broadened water. We note that only one pressure shift has been measured for the rotational band; Golubiatnikov et al. [13] reported a value of $-0.0237 \text{ cm}^{-1} \text{atm}^{-1}$ for the ($3_{13} \leftarrow 2_{20}$) transition which is in excellent agreement with the measured value in v_2 of $-0.0238 (47) \text{ cm}^{-1} \text{atm}^{-1}$. Our measured shift value for ($2_{20} \leftarrow 3_{13}$) is $0.0258 (97) \text{ cm}^{-1} \text{atm}^{-1}$.

In most studies the uncertainties on the half-widths coupled with a relatively small number of data and the lack of measurement for certain types of transitions make it difficult to detect any strong dependence of the half-width on vibration. Studies on HF and HCl indicate that transitions where the energy gap between collisionally coupled levels is large and that have very small broadening values in the ground vibrational state are good candidates to demonstrate the effects of vibration. In 2004, Gamache and Hartmann [64] did a study of water vapor transitions involving levels with $K_c = J$ (or $J - 1$). For such transitions the energy gaps increase quickly with J , and the half-widths decrease by a factor of ~ 20 from $J' = 0$ to $J'' = 18$, a behavior similar to the light hydrogen halides. They showed that the theory predicted large effects of vibration for these lines and were able to confirm this effect using the measurement database [9,72]. The magnitude of the vibrational effect is related to the importance of the vibrational dephasing term, which becomes dominant in far-off resonance collisions. The on/off resonance in the collision

process is given by the matching of the energy jumps of the radiator and perturber in collisionally connected transitions. Thus, the effect of vibration for water vapor transitions will depend on the particular H₂O transition under study and the particular perturbing molecule.

4.8. Approximations to estimate broadening coefficients

For application to planetary radiative transfer studies, all the lines of significant absorption within the spectral range must be known. Unfortunately, there are not enough measurements for H₂O broadened by CO₂ to use Eq. (9) in all the spectral regions needed. Currently the HITRAN database [19] lists 2722 transitions for just the v_2 band of H₂¹⁶O. In this work, the measurements for 256 allowed v_2 transitions between 1287 and 1988 cm^{-1} represents $\sim 90\%$ of the band intensity, but only one forbidden line is measured, and higher J , K_a lines on the wings of the band are not characterized at all. Hence there is a need to approximate the half-widths for the transitions for which there are no direct measurements or calculations for the H₂O–CO₂ system. One simplistic approach is to scale calculated values derived for some other perturbing species [78,79], such as N₂ or air, for which more empirical data are available. In order to test the reliability of this tactic, we divided the present 937 calculated half-widths of the rotation band by the corresponding N₂-broadening half-widths from previous CRB calculations [80]. As shown in the upper panel of Fig. 10, the ratios of $\gamma(\text{CO}_2)/\gamma(\text{N}_2)$ plotted versus $J_m + 0.1 (J_m - K_m)$ vary widely from 0.95 to 3.07 while the average ratio is 1.67, whereas in prior applications [78,79] a ratio of 1.3 was assumed. Clearly, such a

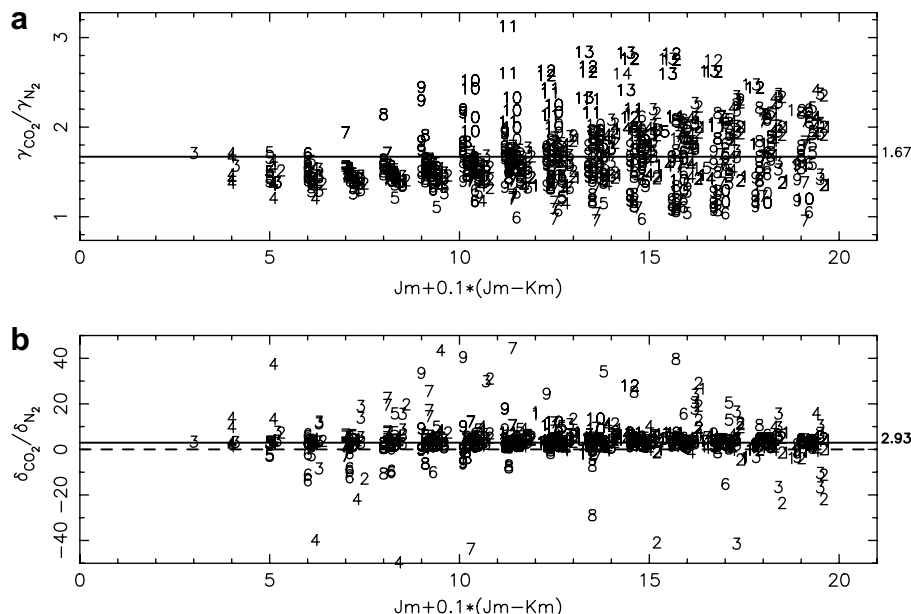


Fig. 10. The ratio of calculated broadening coefficients for ($\text{H}_2\text{O} + \text{CO}_2/\text{H}_2\text{O} + \text{N}_2$) versus $J_m + 0.1(J_m - K_m)$; (a) half-widths (b) pressure shifts. The plot symbol is K_m . A simple scaling of the coefficients for N_2 broadening does not provide a reliable set for CO_2 broadening of water.

scaling will introduce very large errors in the widths. Furthermore, applying this approach to the pressure shifts produces very unreliable results even for the rotational region. The ratios of pressure shifts of all 937 points vary from -525 to $+41799$ with a mean value of $+452$. In Fig. 10b, restricting the ratio values of the shifts in the range from ± 50 , reduces the mean ratio to 4.39. Applying the ratio scheme to near-IR bands is expected to produce even worse coefficients for CO_2 -broadened H_2O .

Using the new measurements and calculations for CO_2 -broadened water, we estimated the magnitude of the line shifts for transitions in the near-IR using Eq. (9). We applied the algorithm of Jacquemart et al. [75] and combined their coefficients for the air-broadened H_2O system with $\text{H}_2\text{O}-\text{CO}_2$ system rotation band line shifts to determine $\text{H}_2\text{O}-\text{CO}_2$ line shifts for transitions at shorter wavelengths. Since the coefficients roughly reflect the vibrational dependence of the radiating molecule (H_2O) and not the perturbing molecule (air or CO_2) it is expected that this procedure will give reasonable estimates. The algorithm was run on the 937 rotational band transitions reported here. For (301)–(000) band at 13830 cm^{-1} , the maximum and minimum line shifts are found to range from 0.050 to $-0.099\text{ cm}^{-1}\text{ atm}^{-1}$ at 296 K. Clearly, such large values the line shifts would impact near infrared retrievals of water vapor in the Venus atmosphere.

5. Conclusions

Empirical half-widths and pressure shifts of water broadened by carbon dioxide at room temperature are obtained for 257 transitions of (010)–(000) between 1287 and 1988 cm^{-1} . Pressure shifts are reported even if the

experimental agreement between measurements are greater than the value itself because estimated precisions for shifts are not always reliable indicators of quality. In addition, the corresponding broadening coefficients (widths, shifts, and temperature dependence of the widths) are calculated for both the rotational and lowest fundamental regions. The mean difference of 2% ($\pm 12\%$) between the observed and calculated widths for the allowed transitions of the (010)–(000) band provides confidence in the calculations, although some systematic differences are seen at higher values of quanta. We note that these checks were made only for allowed transitions of a perpendicular band and that measurements of forbidden transitions and high J transitions are needed to validate the rotational calculation.

This is the first comprehensive measurement of pressure shifts for $\text{H}_2\text{O}-\text{CO}_2$ spectra, and they are observed to be almost as large as those for self-broadening; at room temperature they vary from -0.0386 to $+0.0436\text{ cm}^{-1}\text{ atm}^{-1}$. For the (010)–(000) band, the RMS and mean ratios of the observed and calculated pressure-induced shift coefficients are 1.6 and 0.79, respectively.

Shifts of this magnitude will be very important for interpretation of the spectrum of Venus where the pressures become 90 atm at the surface and temperatures reach 700 K. Thus, more laboratory studies at other wavelengths are needed in order to characterize coefficients for those applications involving Venus and Mars. These include analysis of the temperature dependence of widths, the parameters of parallel type bands and of forbidden transitions (particularly in the (000)–(000) band) and possible line-mixing effects. Simple scaling of existing values of air- or nitrogen-broadened parameters will not achieve sufficiently reliable CO_2 -broadened H_2O coefficients.

The present results for the 937 rotation band transitions of importance to the Mars mission can be found in the [Supplementary Material](#) to this article. It is also available on the web site of the last author (http://faculty.uml.edu/Robert_Gamache).

Acknowledgments

The authors wish to thank the Kitt Peak National Observatory for the use of the FTS. Part of the research de-

scribed in this paper was performed at the Jet Propulsion Laboratory, California Institute of Technology, under contract with The National Aeronautics and Space Administration. RRG and CMH are pleased to acknowledge support of this research by the National Science Foundation through Grant No. ATM-0242537. Any opinions, findings, and conclusions or recommendations expressed in this material are those of the author(s) and do not necessarily reflect the views of the National Science Foundation.

Appendix A

Linewidths (hwhm) and pressure-induced frequency shifts for the ν_2 band of water broadened by carbon dioxide

J'	K'_a	K'_c	J''	K''_a	K''_c	Position (cm^{-1})	obs wid (cm^{-1}) atm $^{-1}$)	% unc	calc wid (cm^{-1}) atm $^{-1}$)	% diff obs.–calc.	obs shift (cm^{-1}) atm $^{-1}$)	unc	calc shift (cm^{-1}) atm $^{-1}$)	Ratio cal./obs.	n	unc
$J_m = 1$																
0	0	0	1	1	1	1557.6092	0.1921	2.2	0.20617	-7.32	-0.02933	123	-0.02886	0.984	0.65	0.021
1	1	1	0	0	0	1634.9671	0.2008	0.7	0.20814	-3.66	0.03322	41	0.02777	0.836	0.67	0.021
1	0	1	1	1	0	1576.1854	0.2101	2.2	0.20811	0.95	-0.02621	76	-0.02583	0.985	0.77	0.027
1	1	0	1	0	1	1616.7115	0.2122	2.1	0.20945	1.30	0.02402	372	0.02664	1.109	0.77	0.023
$J_m = 2$																
1	1	1	2	0	2	1564.8763	0.1804	1.6	0.19666	-9.01	0.01521	85	0.01606	1.056	0.70	0.006
2	0	2	1	1	1	1627.8275	0.1810	1.6	0.19616	-8.38	-0.01218	164	-0.01551	1.273	0.70	0.005
2	1	2	1	0	1	1653.2671	0.1955	2.2	0.19562	-0.06	0.02674	176	0.02515	0.940	0.65	0.021
1	1	0	2	2	1	1505.6043	0.1748	1.5	0.17747	-1.53	0.00072	13	-0.00556	-7.722	0.77	0.026
2	2	1	1	1	0	1699.9339	0.1770	1.8	0.17723	-0.13	0.00217	30	0.00914	4.210	0.77	0.033
1	1	1	2	2	0	1498.8032	0.1717	1.0	0.17908	-4.30	-0.01481	295	-0.01878	1.268	0.69	0.003
2	2	0	1	1	1	1706.3493	0.1688	1.0	0.17723	-4.99	0.01921	134	0.02077	1.081	0.66	0.007
2	1	1	2	0	2	1623.5592	0.2010	2.3	0.20254	-0.77	0.02280	76	0.01931	0.847	0.74	0.012
2	2	1	2	1	2	1662.8093	0.1535	1.2	0.16191	-5.48	0.02287	28	0.02308	1.009	0.56	0.015
2	1	1	2	2	0	1557.4861	0.1755	1.3	0.18271	-4.11	-0.00373	109	-0.00839	2.249	0.72	0.003
2	2	0	2	1	1	1648.3104	0.1784	0.9	0.18406	-3.17	0.00919	46	0.01170	1.274	0.73	0.007
$J_m = 3$																
2	1	2	3	0	3	1540.2998	0.1605	2.5	0.16821	-4.80	0.00811	96	0.00737	0.909	0.52	0.006
3	0	3	2	1	2	1652.4004	0.1577	2.1	0.16814	-6.62	-0.00730	245	-0.00888	1.216	0.49	0.009
2	0	2	3	1	3	1522.6861	0.1702	2.0	0.17773	-4.42	-0.01906	62	-0.01881	0.987	0.68	0.030
3	1	3	2	0	2	1669.3929	0.1732	1.3	0.17750	-2.48	0.01804	48	0.01811	1.004	0.69	0.035
2	2	0	3	1	3	1601.2079	0.1606	4.7	0.16262	-1.26	0.02584	97	0.02659	1.029	0.65	0.028
3	1	3	2	2	0	1603.3198	0.1560	2.7	0.16442	-5.40	-0.02357	466	-0.02432	1.032	0.68	0.030
2	2	1	3	1	2	1568.9399	0.1647	1.9	0.17345	-5.31	0.00731	48	0.00921	1.259	0.64	0.009
3	1	2	2	2	1	1637.5119	0.1598	1.8	0.17068	-6.81	-0.00334	57	-0.00757	2.267	0.60	0.013
2	1	1	3	2	2	1487.3486	0.1644	1.3	0.17370	-5.66	0.00396	32	-0.00050	-0.126	0.71	0.019
3	2	2	2	1	1	1718.6117	0.1669	1.3	0.17540	-5.09	-0.00150	37	0.00319	-2.128	0.74	0.020
2	1	2	3	2	1	1464.9051	0.1723	2.8	0.17706	-2.76	-0.02836	48	-0.02478	0.874	0.63	0.013
3	2	1	2	1	2	1739.8388	0.1653	1.3	0.17471	-5.69	0.03302	146	0.02987	0.905	0.61	0.009
2	2	0	3	3	1	1458.2670	0.1276	1.8	0.13683	-7.23	0.01844	107	0.01315	0.713	0.67	0.014
2	2	1	3	3	0	1456.8870	0.1235	2.3	0.12571	-1.79	-0.00170	146	-0.00070	0.414	0.65	0.038
3	3	0	2	2	1	1772.7142	0.1228	2.3	0.12802	-4.25	-0.00297	84	-0.00394	1.327	0.65	0.027
3	0	3	3	1	2	1558.5309	0.1800	2.4	0.18670	-3.72	-0.01593	22	-0.01407	0.883	0.63	0.010
3	1	2	3	0	3	1635.6519	0.1807	1.3	0.18606	-2.97	0.02406	113	0.01514	0.629	0.64	0.003
3	1	3	3	2	2	1533.1823	0.1263	1.6	0.13877	-9.87	-0.02116	33	-0.02279	1.077	0.57	0.052
3	1	2	3	2	1	1560.2572	0.1712	2.8	0.18062	-5.50	-0.02296	100	-0.01331	0.580	0.62	0.018
3	2	1	3	1	2	1645.9694	0.1729	1.5	0.18094	-4.65	0.01214	199	0.01517	1.250	0.63	0.021
3	3	1	2	2	0	1771.2875	0.1375	1.1	0.14273	-3.80	-0.01553	25	-0.01206	0.776	0.74	0.014
3	2	2	3	3	1	1528.5682	0.1142	1.4	0.12433	-8.87	-0.00873	23	-0.00814	0.933	0.64	0.046
3	3	1	3	2	2	1701.1500	0.1206	1.4	0.12698	-5.29	0.00219	53	0.00321	1.464	0.63	0.043
3	3	0	3	0	3	1770.8542	0.1742	9.4	0.16776	3.70	0.01675	1214	0.02245	1.341	0.69	0.015
3	2	1	3	3	0	1533.9165	0.1416	1.3	0.15035	-6.18	0.01426	23	0.01167	0.819	0.67	0.010
3	3	0	3	2	1	1695.4594	0.1524	0.8	0.15650	-2.69	-0.00937	24	-0.00716	0.764	0.72	0.011

Appendix A (continued)

J'	K'_a	K'_c	J''	K''_a	K''_c	Position (cm^{-1})	obs wid (cm^{-1} atm^{-1})	% unc	calc wid (cm^{-1} atm^{-1})	% diff obs.–calc.	obs shift (cm^{-1} atm^{-1})	unc	calc shift (cm^{-1} atm^{-1})	Ratio cal./obs.	n	unc
$J_m = 4$																
3	1	3	4	0	4	1517.4310	0.1252	1.3	0.13312	-6.33	0.00590	16	0.00305	0.516	0.50	0.051
4	0	4	3	1	3	1675.1727	0.1267	2.4	0.13250	-4.58	-0.00436	40	-0.00305	0.701	0.47	0.055
3	0	3	4	1	4	1507.0583	0.1491	1.9	0.15447	-3.60	-0.01735	34	-0.01762	1.016	0.60	0.015
4	1	4	3	0	3	1684.8352	0.1560	3.3	0.15511	0.57	0.01649	26	0.01511	0.916	0.64	0.020
3	2	1	4	1	4	1594.4968	0.1472	2.4	0.15797	-7.32	0.02347	367	0.02577	1.098	0.69	0.021
4	1	4	3	2	1	1609.4405	0.1539	2.9	0.16202	-5.28	-0.01944	54	-0.01922	0.989	0.73	0.022
3	2	2	4	1	3	1538.2906	0.1523	0.6	0.15918	-4.52	0.00843	604	0.01534	1.820	0.58	0.002
4	1	3	3	2	2	1669.1683	0.1362	1.2	0.15320	-12.48	-0.01744	106	-0.01694	0.971	0.51	0.009
3	1	2	4	2	3	1472.0512	0.1550	1.8	0.16236	-4.75	0.00242	110	0.00027	0.111	0.60	0.005
4	2	3	3	1	2	1734.6506	0.1588	1.5	0.16499	-3.90	0.00051	90	0.00189	3.696	0.65	0.007
3	3	0	4	2	3	1607.2535	0.1175	4.0	0.12842	-9.29	0.01042	211	0.01196	1.147	0.71	0.050
4	2	3	3	3	0	1622.5978	0.1204	1.3	0.12893	-7.08	-0.01681	43	-0.01594	0.948	0.71	0.045
3	1	3	4	2	2	1423.7042	0.1616	0.9	0.16951	-4.89	-0.02301	86	-0.02240	0.973	0.67	0.027
4	2	2	3	1	3	1780.6227	0.1571	2.0	0.16677	-6.16	0.02867	586	0.02892	1.009	0.65	0.024
4	2	2	3	3	1	1637.6818	0.1469	3.2	0.15501	-5.52	0.01466	627	0.01216	0.830	0.67	0.010
3	2	1	4	3	2	1436.8182	0.1395	2.9	0.14595	-4.62	0.02358	76	0.01678	0.712	0.65	0.010
4	3	2	3	2	1	1792.6594	0.1482	2.4	0.15373	-3.73	-0.01691	71	-0.01173	0.694	0.70	0.007
3	2	2	4	3	1	1429.9451	0.1147	1.1	0.12508	-9.05	-0.01863	31	-0.01767	0.948	0.58	0.042
4	3	1	3	2	2	1799.6156	0.1121	1.5	0.12230	-9.10	0.00847	36	0.00991	1.170	0.57	0.050
3	3	0	4	4	1	1419.5080	0.1020	1.8	0.10268	-0.67	0.00781	21	0.00764	0.979	0.79	0.055
4	4	1	3	3	0	1844.1807	0.1073	1.0	0.10999	-2.51	-0.01366	29	-0.01266	0.927	0.74	0.038
3	3	1	4	4	0	1419.3172	0.0994	1.4	0.10152	-2.13	0.00145	51	0.00128	0.880	0.79	0.052
4	4	0	3	3	1	1844.3993	0.1008	2.0	0.10534	-4.50	-0.00633	109	-0.00848	1.339	0.75	0.043
$J_m = 4$																
4	0	4	4	1	3	1541.9542	0.1501	1.5	0.16108	-7.32	0.00421	156	0.00053	0.125	0.53	0.004
4	1	3	4	0	4	1653.4170	0.1384	3.1	0.15353	-10.93	0.00786	240	0.00227	0.289	0.47	0.005
4	1	4	4	2	3	1521.2345	0.1202	2.1	0.12256	-1.96	-0.00719	256	-0.01430	1.989	0.67	0.067
4	2	3	4	1	4	1683.1780	0.1141	1.8	0.12104	-6.08	0.01318	31	0.01419	1.076	0.68	0.067
4	1	3	4	2	2	1559.6902	0.1766	0.9	0.18118	-2.59	-0.02809	65	-0.02066	0.735	0.64	0.006
4	2	2	4	1	3	1647.4041	0.1682	1.0	0.18116	-7.71	0.03025	56	0.02319	0.767	0.66	0.004
4	2	3	4	3	2	1525.4995	0.1080	1.8	0.11500	-6.48	-0.01591	33	-0.01637	1.029	0.68	0.065
4	3	2	4	2	3	1704.4534	0.1079	1.5	0.11656	-8.03	0.00725	25	0.00985	1.358	0.65	0.058
4	3	1	4	2	2	1690.1375	0.1524	1.9	0.15978	-4.84	-0.01251	62	-0.00626	0.501	0.68	0.009
4	3	2	4	4	1	1516.7079	0.1041	1.0	0.11093	-6.56	-0.00212	16	0.00056	-0.263	0.76	0.039
4	4	1	4	3	2	1747.0824	0.1040	2.6	0.11240	-8.08	-0.00394	37	-0.00521	1.322	0.73	0.048
4	4	0	4	3	1	1745.7761	0.1140	1.9	0.12304	-7.93	-0.01239	160	-0.01291	1.042	0.69	0.030
$J_m = 5$																
4	1	4	5	0	5	1496.2489	0.1089	1.8	0.10669	2.03	0.00174	55	-0.00162	-0.930	0.62	0.088
5	0	5	4	1	4	1695.9282	0.1111	3.9	0.10673	3.93	0.00134	21	0.00431	3.218	0.60	0.087
4	0	4	5	1	5	1490.8257	0.1160	1.0	0.12517	-7.91	-0.01678	29	-0.01783	1.063	0.61	0.047
5	1	5	4	0	4	1700.7763	0.1215	1.4	0.12681	-4.37	0.01678	65	0.01594	0.950	0.62	0.039
5	1	5	4	2	2	1607.0495	0.1542	1.2	0.16222	-5.20	-0.00391	374	-0.01609	4.115	0.72	0.013
4	2	3	5	1	4	1508.5588	0.1343	1.3	0.14420	-7.37	0.02421	126	0.01977	0.817	0.62	0.015
5	1	4	4	2	3	1700.5008	0.1313	1.0	0.14086	-7.28	-0.02674	40	-0.02311	0.864	0.58	0.027
4	1	3	5	2	4	1459.2610	0.1336	1.6	0.14852	-11.17	-0.01456	50	-0.01254	0.862	0.55	0.008
5	2	4	4	1	3	1748.6557	0.1455	2.0	0.15627	-7.40	0.01494	31	0.01137	0.761	0.63	0.003
4	3	1	5	2	4	1589.7083	0.1144	5.3	0.12391	-8.31	0.01809	171	0.01946	1.076	0.70	0.045
5	2	4	4	3	1	1640.3102	0.1200	2.9	0.12847	-7.06	-0.01167	558	-0.02126	1.822	0.68	0.029
5	2	4	5	1	5	1697.5272	0.1044	1.4	0.11076	-6.09	0.00690	41	0.00893	1.294	0.77	0.060
4	1	4	5	2	3	1375.0862	0.1475	2.3	0.15827	-7.30	-0.02252	94	-0.01995	0.886	0.63	0.018
5	2	3	4	1	4	1829.1304	0.1426	1.9	0.15425	-8.17	0.03168	76	0.02724	0.860	0.63	0.022
4	2	2	5	3	3	1418.9330	0.1438	0.9	0.14985	-4.21	0.02704	71	0.01665	0.616	0.66	0.009
5	3	3	4	2	2	1810.6282	0.1525	1.1	0.15696	-2.92	-0.01716	47	-0.01196	0.697	0.70	0.008
4	2	3	5	3	2	1399.2042	0.1257	1.0	0.13284	-5.68	-0.02673	32	-0.02506	0.938	0.63	0.028
5	3	2	4	2	3	1830.1320	0.1162	1.5	0.12597	-8.41	0.01998	33	0.02080	1.041	0.64	0.051
5	3	2	4	4	1	1642.3865	0.1156	5.1	0.12541	-8.49	0.01026	228	0.01163	1.133	0.72	0.035
4	3	1	5	4	2	1395.8026	0.1008	2.2	0.10946	-8.59	0.01430	47	0.01469	1.027	0.70	0.045
5	4	2	4	3	1	1867.8528	0.1104	1.6	0.11945	-8.20	-0.01957	91	-0.01721	0.880	0.68	0.031
4	3	2	5	4	1	1394.4744	0.0991	1.1	0.09794	1.17	-0.00151	131	-0.00277	1.834	0.63	0.037
5	4	1	4	3	2	1869.3457	0.0986	1.0	0.10307	-4.53	-0.00723	30	-0.00762	1.054	0.67	0.058
4	4	0	5	5	1	1387.5456	0.0937	4.7	0.08475	9.55	0.00018	25	0.00098	5.444	0.89	0.049

(continued on next page)

Appendix A (continued)

J'	K'_a	K'_c	J''	K''_a	K''_c	Position (cm^{-1})	obs wid (cm^{-1} atm^{-1})	% unc	calc wid (cm^{-1} atm^{-1})	% diff obs.–calc.	obs shift (cm^{-1} atm^{-1})	unc	calc shift (cm^{-1} atm^{-1})	Ratio cal./obs.	n	unc
4	4	1	5	5	0	1387.5229	0.0909	3.0	0.08480	6.71	0.00094	97	-0.00022	-0.231	0.89	0.048
5	5	0	4	4	1	1918.0354	0.0962	4.0	0.08716	9.39	-0.01212	524	-0.00753	0.622	0.84	0.050
5	0	5	5	1	4	1521.3091	0.1321	2.7	0.14219	-7.64	0.01543	376	0.01316	0.853	0.59	0.014
5	1	4	5	0	5	1675.5151	0.1238	1.1	0.13644	-10.21	-0.01545	27	-0.01455	0.942	0.56	0.025
5	1	5	5	2	4	1506.6203	0.1072	3.1	0.11107	-3.61	-0.00452	43	-0.00775	1.715	0.75	0.064
5	1	4	5	2	3	1554.3524	0.1634	1.8	0.16874	-3.27	-0.03608	50	-0.02786	0.772	0.59	0.008
5	2	3	5	1	4	1654.5112	0.1624	1.2	0.17062	-5.06	0.03816	21	0.03084	0.808	0.63	0.010
5	3	3	5	2	4	1710.1990	0.1019	1.7	0.11012	-8.07	0.00949	52	0.01386	1.460	0.73	0.061
5	2	3	5	3	2	1545.1566	0.1288	1.6	0.14776	-14.72	0.00870	21	0.00631	0.726	0.51	0.011
5	3	2	5	2	3	1683.9837	0.1384	1.7	0.15390	-11.20	-0.01075	36	-0.00354	0.329	0.56	0.008
5	3	3	5	4	2	1516.2933	0.0941	1.9	0.09997	-6.24	-0.00378	37	-0.00550	1.456	0.74	0.057
5	4	2	5	3	3	1747.7272	0.1011	4.0	0.10511	-3.97	-0.00532	91	-0.00466	0.876	0.75	0.058
5	3	2	5	4	1	1520.1530	0.1130	1.0	0.11869	-5.04	0.01733	561	0.01358	0.784	0.69	0.040
5	4	2	5	5	1	1509.6222	0.0936	2.2	0.10339	-10.46	-0.00045	90	0.00231	-5.137	0.84	0.027
5	5	1	5	4	2	1796.0265	0.1034	2.8	0.10318	0.21	-0.00066	493	-0.00589	8.930	0.80	0.036
5	5	0	5	4	1	1795.8019	0.1005	2.1	0.10558	-5.05	-0.00512	166	-0.00762	1.488	0.80	0.033
$J_m = 6$																
5	1	5	6	0	6	1476.1325	0.0940	1.3	0.08809	6.29	-0.00030	22	-0.00796	26.531	0.71	0.089
6	0	6	5	1	5	1715.1551	0.0934	0.8	0.08913	4.57	0.00269	19	0.01169	4.345	0.68	0.082
5	0	5	6	1	6	1473.5142	0.0994	1.7	0.09986	-0.46	-0.01241	32	-0.02238	1.804	0.72	0.076
6	1	6	5	0	5	1717.4055	0.1054	2.9	0.10320	2.09	0.01291	30	0.02080	1.612	0.71	0.064
5	2	4	6	1	5	1481.2469	0.1170	1.1	0.12731	-8.81	0.02401	57	0.02235	0.931	0.65	0.027
6	1	5	5	2	4	1730.0550	0.1132	2.0	0.12491	-10.34	-0.02255	305	-0.02437	1.080	0.63	0.038
5	1	4	6	2	5	1447.9516	0.1267	1.2	0.13730	-8.37	-0.02520	46	-0.02232	0.886	0.60	0.017
6	2	5	5	1	4	1761.8286	0.1362	1.5	0.14355	-5.40	0.02284	45	0.01917	0.839	0.64	0.008
5	3	2	6	2	5	1577.5829	0.1137	4.8	0.12560	-10.47	0.02201	222	0.02302	1.046	0.67	0.033
5	1	5	6	2	4	1320.0556	0.1186	2.6	0.13847	-16.75	-0.00658	192	-0.00754	1.147	0.54	0.029
6	2	4	5	3	3	1707.2225	0.1052	3.4	0.12262	-16.56	0.00859	62	0.00563	0.656	0.49	0.051
5	2	3	6	3	4	1404.9900	0.1309	0.9	0.14367	-9.76	0.02592	37	0.01754	0.677	0.60	0.013
6	3	4	5	2	3	1825.2017	0.1394	1.1	0.15004	-7.63	-0.01456	205	-0.01076	0.739	0.60	0.004
5	4	1	6	3	4	1602.8838	0.1042	2.5	0.10912	-4.72	-0.00045	333	0.00130	-2.880	0.79	0.045
6	3	4	5	4	1	1661.3710	0.1023	2.3	0.10877	-6.32	-0.00446	214	-0.00682	1.529	0.79	0.040
5	2	4	6	3	3	1362.6037	0.1279	3.4	0.13904	-8.71	-0.02070	849	-0.02809	1.357	0.63	0.014
6	3	3	5	2	4	1866.3809	0.1259	3.9	0.13155	-4.49	0.02744	166	0.02826	1.030	0.63	0.030
5	3	2	6	4	3	1373.7695	0.1072	1.3	0.11640	-8.58	0.01722	48	0.01664	0.967	0.68	0.041
6	4	3	5	3	2	1889.5695	0.1208	1.4	0.12820	-6.13	-0.01974	444	-0.02148	1.088	0.64	0.021
5	3	3	6	4	2	1368.6275	0.0959	1.8	0.09946	-3.71	-0.00837	67	-0.01426	1.704	0.70	0.064
6	4	2	5	3	3	1895.1974	0.0956	3.6	0.10251	-7.23	-0.00497	123	-0.00574	1.155	0.72	0.058
5	4	1	6	5	2	1363.2637	0.0919	0.9	0.09053	1.49	0.00422	36	0.00732	1.735	0.80	0.036
6	5	2	5	4	1	1942.5161	0.0953	1.6	0.09523	0.07	-0.00961	42	-0.01334	1.388	0.76	0.038
6	5	1	5	4	2	1942.7654	0.0953	4.5	0.09054	4.99	-0.00741	150	-0.00958	1.293	0.75	0.043
6	0	6	6	1	5	1498.8748	0.1139	0.9	0.12379	-8.68	0.01314	760	0.02028	1.543	0.64	0.028
6	1	5	6	0	6	1699.5672	0.1114	2.8	0.12115	-8.75	-0.01955	149	-0.02195	1.123	0.64	0.036
6	1	6	6	2	5	1489.8420	0.0997	1.0	0.10088	-1.18	-0.00202	17	-0.00370	1.830	0.79	0.056
6	2	5	6	1	6	1714.0337	0.0986	1.2	0.10153	-2.97	0.00355	21	0.00546	1.537	0.83	0.049
6	1	5	6	2	4	1543.4903	0.1264	1.4	0.14205	-12.38	-0.02502	44	-0.02113	0.845	0.49	0.026
6	2	4	6	1	5	1668.2849	0.1295	2.3	0.14259	-10.11	0.03688	91	0.03001	0.814	0.54	0.030
6	3	4	6	2	5	1718.8009	0.1022	1.6	0.10785	-5.53	0.01281	77	0.01681	1.312	0.77	0.045
6	2	4	6	3	3	1549.6417	0.1255	1.8	0.14214	-13.26	-0.02748	29	-0.01995	0.726	0.49	0.029
6	3	3	6	2	4	1679.8162	0.1248	2.4	0.14436	-15.67	0.02028	109	0.01980	0.977	0.50	0.026
6	3	4	6	4	3	1514.9875	0.0945	1.1	0.09704	-2.69	-0.00586	12	-0.00780	1.332	0.79	0.059
6	4	3	6	3	4	1749.4028	0.0954	2.2	0.09899	-3.77	-0.00549	46	-0.00651	1.186	0.73	0.056
6	3	3	6	4	2	1524.8094	0.1117	1.7	0.12498	-11.89	0.01842	292	0.01897	1.030	0.65	0.036
6	4	2	6	3	3	1737.6166	0.1288	2.7	0.13668	-6.12	-0.02148	527	-0.02279	1.061	0.63	0.012
6	5	2	6	4	3	1796.1325	0.0973	1.9	0.09668	0.64	-0.00305	219	-0.00752	2.464	0.83	0.051
6	4	2	6	5	1	1510.5328	0.0901	3.1	0.09982	-10.79	0.00157	238	0.00268	1.705	0.80	0.028
6	5	1	6	4	2	1795.0996	0.0953	3.6	0.10397	-9.10	-0.00529	331	-0.01158	2.190	0.77	0.044
$J_m = 7$																
6	1	6	7	0	7	1456.5098	0.0872	0.9	0.07213	17.28	-0.00171	20	-0.01144	6.689	0.75	0.085
7	0	7	6	1	6	1733.3906	0.0881	1.9	0.07286	17.30	0.00336	19	0.01532	4.559	0.72	0.083

Appendix A (continued)

J'	K'_a	K'_c	J''	K''_a	K''_c	Position (cm^{-1})	obs wid (cm^{-1} atm^{-1})	% unc	calc wid (cm^{-1} atm^{-1})	% diff obs.–calc.	obs shift (cm^{-1} atm^{-1})	unc	calc shift (cm^{-1} atm^{-1})	Ratio cal./obs.	n	unc
6	0	6	7	1	7	1455.3014	0.0849	1.4	0.07356	13.36	-0.00793	28	-0.02059	2.596	0.69	0.080
7	1	7	6	0	6	1734.3934	0.0892	1.0	0.07768	12.92	0.00896	51	0.02238	2.498	0.68	0.067
6	2	5	7	1	6	1457.0720	0.1042	1.0	0.11186	-7.35	0.01434	232	0.02322	1.619	0.78	0.055
7	1	6	6	2	5	1756.8189	0.0996	1.3	0.11042	-10.86	-0.01988	31	-0.02673	1.345	0.80	0.067
6	1	5	7	2	6	1436.6555	0.1124	2.2	0.12263	-9.10	-0.01881	552	-0.02488	1.323	0.65	0.027
7	2	6	6	1	5	1775.6342	0.1166	0.8	0.12587	-7.95	0.02531	41	0.02369	0.936	0.65	0.019
7	2	5	6	1	6	1945.3403	0.1069	4.0	0.11856	-10.91	-0.00464	151	-0.00598	1.289	0.62	0.060
6	3	4	7	2	5	1489.3024	0.1154	2.0	0.13104	-13.55	0.02355	65	0.02205	0.936	0.60	0.031
7	3	5	6	2	4	1837.1810	0.1156	2.0	0.13197	-14.16	0.00477	96	0.00527	1.106	0.48	0.017
6	2	5	7	3	4	1318.9294	0.1266	2.8	0.13716	-8.34	-0.02959	131	-0.02705	0.914	0.62	0.014
7	3	4	6	2	5	1909.9640	0.1216	1.9	0.13090	-7.65	0.03308	137	0.03159	0.955	0.61	0.023
7	3	4	6	4	3	1706.1505	0.1137	3.7	0.12544	-10.33	0.02052	641	0.02416	1.177	0.63	0.033
6	3	3	7	4	4	1354.8457	0.1104	2.6	0.12383	-12.16	0.02130	423	0.02062	0.968	0.65	0.030
6	3	4	7	4	3	1340.4751	0.1011	2.2	0.10982	-8.63	-0.01407	115	-0.02091	1.486	0.75	0.051
7	5	3	6	4	2	1966.2613	0.0968	2.3	0.10290	-6.30	-0.00966	394	-0.02046	2.118	0.76	0.044
6	4	3	7	5	2	1338.5460	0.0869	3.2	0.08493	2.26	-0.00409	131	-0.00463	1.133	0.68	0.038
7	5	2	6	4	3	1967.4424	0.0931	2.5	0.09368	-0.63	-0.01006	47	-0.01485	1.476	0.81	0.052
7	0	7	7	1	6	1476.4289	0.0998	1.0	0.10692	-7.13	0.01586	34	0.02263	1.427	0.73	0.045
7	1	6	7	0	7	1723.4867	0.0980	2.0	0.10654	-8.71	-0.01612	39	-0.02392	1.484	0.75	0.046
7	1	7	7	2	6	1471.4817	0.0953	1.4	0.09062	4.91	0.00009	20	-0.00025	-2.810	0.81	0.051
7	2	6	7	1	7	1732.0608	0.0944	3.8	0.09264	1.86	0.00221	250	0.00241	1.090	0.86	0.043
7	1	6	7	2	5	1527.3204	0.1080	1.3	0.12222	-13.17	0.00242	19	0.00625	2.582	0.49	0.042
7	2	5	7	1	6	1688.3785	0.1016	1.6	0.11163	-9.87	0.01175	42	0.00796	0.677	0.52	0.073
7	2	6	7	3	5	1501.8456	0.0927	2.0	0.10001	-7.89	-0.01011	50	-0.01809	1.789	0.76	0.039
7	3	5	7	2	6	1730.3463	0.0949	2.3	0.10265	-8.17	0.01364	160	0.02005	1.470	0.80	0.037
7	2	5	7	3	4	1550.2360	0.1328	1.5	0.14381	-8.29	-0.03805	71	-0.03177	0.835	0.57	0.033
7	3	4	7	2	5	1680.4655	0.1295	2.3	0.14621	-12.90	0.03961	113	0.03556	0.898	0.55	0.024
7	3	5	7	4	4	1512.2105	0.0929	2.0	0.09570	-3.01	-0.00417	295	-0.01312	3.147	0.76	0.034
7	4	4	7	3	5	1752.8137	0.0913	4.3	0.09194	-0.70	0.00226	187	0.00485	2.147	0.74	0.057
7	3	4	7	4	3	1531.6381	0.1028	1.0	0.12347	-20.11	0.01909	68	0.01896	0.993	0.61	0.047
7	4	3	7	3	4	1729.7826	0.1265	1.9	0.13387	-5.83	-0.02068	354	-0.01999	0.967	0.59	0.021
7	5	3	7	4	4	1796.2976	0.0914	4.7	0.09765	-6.84	-0.00288	345	-0.01622	5.633	0.83	0.039
7	5	2	7	4	3	1792.9300	0.1106	2.8	0.11261	-1.82	-0.01198	582	-0.02178	1.818	0.78	0.044
7	5	2	7	6	1	1507.9726	0.0864	5.6	0.09207	-6.57	-0.00238	114	-0.00203	0.854	0.84	0.016
$J_m = 8$																
7	1	7	8	0	8	1437.0262	0.0808	2.0	0.05880	27.23	-0.00168	89	-0.01202	7.155	0.72	0.074
8	0	8	7	1	7	1750.9842	0.0758	2.7	0.05967	21.28	0.00157	164	0.01526	9.720	0.72	0.076
7	0	7	8	1	8	1436.4802	0.0784	0.7	0.05734	26.86	-0.00491	81	-0.01453	2.958	0.69	0.076
8	1	8	7	0	7	1751.4233	0.0822	1.7	0.05943	27.70	0.00743	30	0.01779	2.395	0.66	0.071
7	2	6	8	1	7	1435.6496	0.0885	2.5	0.08780	0.79	0.00997	182	0.02374	2.381	0.80	0.063
7	1	6	8	2	7	1424.1300	0.0969	1.3	0.11262	-16.22	-0.02163	49	-0.03187	1.473	0.85	0.053
8	2	7	7	1	6	1790.9518	0.0999	1.8	0.11272	-12.83	0.02033	29	0.02787	1.371	0.82	0.050
7	2	5	8	3	6	1386.4766	0.0940	0.7	0.11574	-23.13	-0.01525	342	-0.02295	1.505	0.65	0.076
8	3	6	7	2	5	1847.7828	0.1136	1.9	0.12952	-14.01	0.02695	55	0.02190	0.812	0.59	0.029
8	3	5	8	2	6	1687.8780	0.1235	4.9	0.13755	-11.38	0.04364	190	0.03918	0.898	0.59	0.034
7	3	4	8	4	5	1340.1668	0.1089	3.2	0.12358	-13.48	0.02465	592	0.02420	0.982	0.61	0.029
8	4	5	7	3	4	1922.3409	0.1190	1.1	0.13241	-11.27	-0.01877	646	-0.02171	1.156	0.60	0.018
8	4	4	7	3	5	1954.9959	0.0972	3.4	0.10868	-11.81	0.01483	299	0.02445	1.649	0.78	0.059
7	4	3	8	5	4	1316.9724	0.0959	1.2	0.09341	2.59	0.00634	139	0.00717	1.130	0.70	0.038
8	5	4	7	4	3	1988.3959	0.1007	3.0	0.11036	-9.59	-0.01542	260	-0.02511	1.628	0.77	0.049
7	5	2	8	6	3	1312.5557	0.0950	4.2	0.08375	11.84	-0.00245	141	-0.00339	1.384	0.77	0.021
8	0	8	8	1	7	1454.5730	0.0880	4.9	0.08890	-1.03	0.00808	150	0.02265	2.803	0.77	0.047
8	1	7	8	0	8	1746.2904	0.0828	4.3	0.08901	-7.50	-0.00608	233	-0.02410	3.964	0.79	0.045
8	1	8	8	2	7	1452.0666	0.0898	0.6	0.08113	9.65	0.00005	41	0.00257	51.406	0.84	0.048
8	2	6	8	1	7	1712.9226	0.0921	2.1	0.10948	-18.87	-0.00860	247	-0.02217	2.578	0.66	0.062
8	2	7	8	3	6	1489.0499	0.0882	1.4	0.08739	0.92	-0.00711	31	-0.01626	2.287	0.76	0.046
8	3	6	8	2	7	1744.5924	0.0897	2.0	0.09287	-3.53	0.01279	99	0.02206	1.724	0.80	0.032
8	2	6	8	3	5	1545.6553	0.1240	3.6	0.13443	-8.41	-0.02190	907	-0.03446	1.574	0.57	0.040
8	3	6	8	4	5	1507.4841	0.0819	3.8	0.08851	-8.07	-0.00944	689	-0.02027	2.148	0.67	0.032
8	4	5	8	3	6	1758.5815	0.0912	2.3	0.09129	-0.10	0.01093	173	0.02108	1.929	0.81	0.056

(continued on next page)

Appendix A (continued)

J'	K'_a	K'_c	J''	K''_a	K''_c	Position (cm^{-1})	obs wid (cm^{-1} atm^{-1})	% unc	calc wid (cm^{-1} atm^{-1})	% diff obs.–calc.	obs shift (cm^{-1} atm^{-1})	unc	calc shift (cm^{-1} atm^{-1})	Ratio cal./obs.	n	unc
8	4	4	8	3	5	1721.5325	0.1030	3.1	0.11679	–13.39	–0.00012	234	–0.00710	59.169	0.45	0.033
8	4	5	8	5	4	1509.5307	0.0843	4.3	0.08409	0.25	–0.00026	126	0.00065	–2.490	0.77	0.031
8	5	4	8	4	5	1796.9244	0.0889	4.4	0.08976	–0.97	–0.00655	271	–0.01696	2.589	0.75	0.040
$J_m = 9$																
8	1	8	9	0	9	1417.4985	0.0698	0.9	0.04897	29.84	–0.00266	28	–0.01036	3.894	0.65	0.056
9	0	9	8	1	8	1768.1202	0.0714	0.9	0.04970	30.40	0.00438	30	0.01269	2.896	0.67	0.059
8	0	8	9	1	9	1417.2532	0.0693	1.8	0.04805	30.67	–0.00434	22	–0.01017	2.344	0.65	0.060
9	1	9	8	0	8	1768.3120	0.0724	0.5	0.04895	32.39	0.00569	92	0.01326	2.331	0.64	0.062
8	2	7	9	1	8	1416.0863	0.0853	0.8	0.06783	20.48	0.00844	81	0.01180	1.398	0.79	0.061
9	1	8	8	2	7	1802.4797	0.0810	1.7	0.06036	25.48	–0.00922	41	–0.01115	1.209	0.63	0.057
9	2	8	8	1	7	1807.7033	0.0900	3.1	0.08667	3.70	0.01366	98	0.03428	2.510	0.78	0.049
8	3	6	9	2	7	1428.2711	0.0989	1.5	0.11899	–20.31	0.02590	79	0.02663	1.028	0.79	0.045
9	2	7	8	3	6	1812.2822	0.1016	2.1	0.11918	–17.30	–0.02901	70	–0.03017	1.040	0.86	0.056
9	3	6	8	4	5	1781.9619	0.0919	6.6	0.09282	–1.01	–0.00021	130	0.00710	–33.829	0.50	0.061
8	4	5	9	5	4	1287.4001	0.0903	1.1	0.08370	7.31	–0.00647	289	–0.01779	2.750	0.64	0.020
9	0	9	9	1	8	1433.2033	0.0839	1.7	0.07305	12.94	0.00474	57	0.01631	3.440	0.83	0.052
9	1	8	9	0	9	1767.9116	0.0912	5.3	0.07286	20.12	–0.00290	158	–0.01730	5.965	0.84	0.050
9	1	8	9	2	7	1486.1584	0.0915	1.6	0.10756	–17.55	0.01917	57	0.02927	1.527	0.76	0.053
9	2	7	9	1	8	1739.3185	0.0998	1.7	0.10620	–6.41	–0.00612	558	–0.03003	4.907	0.76	0.048
9	2	8	9	3	7	1474.3623	0.0808	6.5	0.07614	5.76	–0.00107	121	–0.01250	11.686	0.80	0.059
9	2	7	9	3	6	1535.4790	0.1024	3.1	0.11733	–14.58	–0.02398	124	–0.02260	0.942	0.68	0.087
9	3	6	9	2	7	1702.7489	0.1073	4.6	0.11865	–10.58	0.03253	163	0.02910	0.894	0.63	0.048
9	3	6	9	4	5	1544.4351	0.0987	2.3	0.11843	–19.99	–0.02268	344	–0.02422	1.068	0.69	0.078
$J_m = 10$																
9	1	9	10	0	10	1397.8434	0.0613	3.8	0.04221	31.14	–0.00230	86	–0.00828	3.600	0.59	0.047
10	0	10	9	1	9	1784.8869	0.0627	1.5	0.04278	31.77	0.00429	57	0.01005	2.342	0.59	0.046
9	0	9	10	1	10	1397.7330	0.0611	2.1	0.04201	31.25	–0.00356	62	–0.00813	2.285	0.59	0.048
10	1	10	9	0	9	1784.9713	0.0645	1.2	0.04245	34.19	0.00613	32	0.01004	1.638	0.59	0.048
9	2	8	10	1	9	1397.5755	0.0809	9.2	0.05726	29.22	0.00249	333	0.00024	0.095	0.77	0.053
10	1	9	9	2	8	1822.7606	0.0755	2.6	0.05100	32.44	–0.00496	150	0.00066	–0.134	0.64	0.053
10	2	9	9	1	8	1825.3488	0.0840	2.0	0.06188	26.33	0.00972	78	0.02586	2.660	0.73	0.055
10	3	8	9	2	7	1870.8049	0.1088	4.2	0.11982	–10.13	0.02644	528	0.02853	1.079	0.85	0.053
10	3	8	10	4	7	1491.3903	0.0728	6.5	0.06581	9.60	–0.01077	154	–0.02135	1.983	0.62	0.059
$J_m = 11$																
10	1	10	11	0	11	1378.0296	0.0539	4.2	0.03795	29.60	–0.00150	123	–0.00905	6.033	0.53	0.041
11	0	11	10	1	10	1801.3245	0.0552	1.6	0.03831	30.60	0.00446	70	0.01012	2.268	0.53	0.040
11	1	11	10	0	10	1801.3621	0.0575	1.7	0.03823	33.52	0.00396	196	0.00999	2.522	0.53	0.040
11	1	10	10	2	9	1842.1307	0.0682	1.8	0.04494	34.11	–0.00206	149	0.00701	–3.401	0.64	0.054
11	2	9	10	3	8	1868.7274	0.0893	0.5	0.06878	22.98	–0.02106	268	–0.04683	2.224	0.70	0.052
11	2	9	11	3	8	1501.6322	0.0883	1.8	0.10043	–13.74	0.01397	470	0.03147	2.252	0.72	0.057
$J_m = 12 \& 13$																
12	1	12	11	0	11	1817.4688	0.0506	3.6	0.03527	30.29	0.00387	302	0.01203	3.109	0.50	0.045
11	1	10	12	2	11	1361.0135	0.0634	5.7	0.03663	42.23	–0.00873	465	–0.01115	1.277	0.42	0.022
13	0	13	12	1	12	1833.2784	0.0450	7.8	0.03147	30.07	0.00093	291	0.00753	8.092	0.41	0.046

Appendix B. Supplementary data

Supplementary data for this article are available on ScienceDirect (www.sciencedirect.com) and as part of the Ohio State University Molecular Spectroscopy Archives (http://msa.lib.ohio-state.edu/jmsa_hp.htm).

References

- [1] D.V. Titov, H. Svedhem, D. McCoy D, J.-P. Lebreton, S. Barabash, J. -L. Bertaux, P. Drossart, V. Formisano, B. Haeusler, O.I. Korablev, W. Markiewicz, D. Neveance, M. Petzold, G. Piccioni, T.L. Zhang, F.W. Taylor, E. Lellouch, D. Koschny, O. Witasse, M.M. Warhaut, A. Acomazzo, J. Rodrigues-Cannabal, J. Fabrega, T. Schirmann, A. Clochet, M. Coradini, *Cosmic Res.* 44 (2006) 334–348.
- [2] E. Ammannito, G. Filacchione, A. Coradini, F. Capaccioni, G. Piccioni, M.C. De Sanctis, M. Dami, A. Barbis, *Rev. Sci. Instrum.* 77 (2006). Art. No. 093109..
- [3] J.E. Graf, R.W. Zurek, H.J. Eisen, B. Jaum, M.D. Johnston, R. DePaula, *Acta Astronautica.* 57 (2005) 566–578.
- [4] D.J. McCleese, J.T. Schofield, F.W. Taylor, S. Calcutt, M. Foote, D. M. Kass, C.B. Leovy, D.A. Paige, P.L. Read, R.W. Zurek, *J. Geophys. Res.* doi:10.1029/2006JE002790.
- [5] F.W. Taylor, *Adv. Space Res.* 36 (2005) 2138–2141.

- [6] D.H. Grinspoon, M.A. Bullock, *Geochim Cosmochim Acta* 69 (2005) A750, Suppl. S.
- [7] A. Fedorova, O. Korablev, J.-L. Bertaux, A. Rodin, A. Kiselev, S. Perrier, *J. Geophys. Res.-Planets* 111 (2006). Art. No. E09S08..
- [8] A.L. Sprague, D.M. Hunten, L.R. Doose, R.E. Hill, W.V. Boynton, M.D. Smith, J.C. Pearl, *Icarus* 184 (2006) 372–400.
- [9] R.R. Gamache, J.-M. Hartmann, L. Rosenmann, *J. Quant. Spectrosc. Radiat. Transfer* 52 (1994) 481–499.
- [10] J.R. Izatt, H. Sakai, W.S. Benedict, *J. Opt. Soc. Am.* 59 (1969) 19–26.
- [11] P. Varanasi, C.R. Prasad, *J. Quant. Spectrosc. Radiat. Transfer* 10 (1970) 65–69.
- [12] P. Varanasi, *J. Quant. Spectrosc. Radiat. Transfer* 11 (1971) 223–230.
- [13] G.Y. Golubiatnikov, *J. Mol. Spectrosc.* 230 (2005) 196–198.
- [14] L.R. Brown, D.C. Benner, V.M. Devi, M.A.H. Smith, R.A. Toth, *J. Mol. Struct.* 742 (2005) 111–122.
- [15] R.R. Gamache, S.P. Neshyba, J.J. Plateaux, A. Barbe, L. Regalia, J.B. Pollack, *J. Mol. Spectrosc.* 170 (1995) 131–151.
- [16] V. Nagali, S.I. Chou, D.S. Baer, R.K. Hanson, *J. Quant. Spectrosc. Radiat. Transfer* 57 (1997) 795–809.
- [17] S. Langlois, T.P. Birbeck, R.K. Hanson, *J. Mol. Spectrosc.* 167 (1994) 272–282.
- [18] R.R. Gamache, R. Lynch, J.J. Plateaux, A. Barbe, *J. Quant. Spectrosc. Radiat. Transfer* 57 (1997) 485–496.
- [19] D. Robert, J. Bonamy, *J. Physique* 20 (1979) 923–943.
- [20] L.S. Rothman, D. Jacquemart, A. Barbe, D.C. Benner, M. Birk, L.R. Brown, M.R. Carleer, C. Chackerian Jr, K. Chance, V. Dana, V.M. Devi, J.-M. Flaud, R.R. Gamache, A. Goldman, J.-M. Hartmann, K.W. Jucks, A.G. Maki, J.-Y. Mandin, S. Massie, J. Orphal, A. Perrin, C.P. Rinsland, M.A.H. Smith, R.A. Toth, J. Vander Auwera, P. Varanasi, G. Wagner, *J. Quant. Spectrosc. Radiat. Transfer* 92 (2005) 139–207.
- [21] D. Lisak, J.T. Hodges, R. Ciurylo, *Phys. Rev. A* 73 (2006). Art. No. 012507..
- [22] L.R. Brown, J.S. Margolis, R.H. Norton, B.D. Stedry, *Appl. Spectrosc.* 37 (1983) 287–292.
- [23] R.A. Toth, *J. Mol. Spectrosc.* 190 (1998) 379–396.
- [24] R.A. Toth, L.R. Brown, C. Plymate, *J. Quant. Spectrosc. Radiat. Transfer* 59 (1998) 529–562.
- [25] A.G. Maki, J.S. Wells, *J. Res. Nat. Instit. Stand. Technol.* 97 (1992) 409–470.
- [26] R.A. Toth, L.R. Brown, C.E. Miller, V.M. Devi, D.C. Benner, *J. Mol. Spectrosc.* 239 (2006) 229–249.
- [27] L.R. Brown, C. Plymate, *J. Mol. Spectrosc.* 100 (2000) 166–179.
- [28] P. Varanasi, G.T.D. Tejwani, C.R. Prasad, *J. Quant. Spectrosc. Radiat. Transfer* 11 (1971) 231–236.
- [29] P.W. Anderson, Dissertation, Harvard University, 1949.
- [30] P.W. Anderson, *Phys. Rev.* 76 (1949) 647–661.
- [31] P.W. Anderson, *Phys. Rev.* 80 (1950) 511–513.
- [32] C.J. Tsao, B. Curnutte Jr., *J. Quant. Spectrosc. Radiat. Transfer* 2 (1962) 41–91.
- [33] C. Delaye, J.-M. Hartmann, J. Taine, *Appl. Opt.* 28 (1989) 5080–5087.
- [34] R.R. Gamache, R. Lynch, S.P. Neshyba, *J. Quant. Spectrosc. Radiat. Transfer* 59 (1998) 319–335.
- [35] R. Lynch, R.R. Gamache, S.P. Neshyba, *J. Quant. Spectrosc. Radiat. Transfer* 59 (1998) 595–613.
- [36] R. Lynch, Ph.D. Dissertation, Physics Department, University of Massachusetts Lowell, 1995.
- [37] R. Kubo, *J. Phys. Soc. Japan* 17 (1962) 1100–1120.
- [38] J.E. Jones, *Proc. R. Soc. A* 106 (1924) 463–477.
- [39] S.P. Neshyba, R. Lynch, R.R. Gamache, T. Gabard, J.-P. Champion, *J. Chem. Phys.* 101 (1994) 9412–9421.
- [40] R.R. Gamache, N. Lacombe, G. Pierre, T. Gabard, *J. Mol. Struct.* 599 (2001) 279–292.
- [41] T. Oka, Academic Press, New York, 1973.
- [42] M. Baranger, *Phys. Rev.* 112 (1958) 855–865.
- [43] A. Ben-Reuven, Spectral Line Shapes in Gases in the Binary-Collision Approximation, in: I.P.a.S.A. Rice (Ed.), *Adv. Chem. Phys.*, Academic Press, New York, 1975, p. 235.
- [44] S.L. Shostak, J.S. Muentzer, *J. Chem. Phys.* 94 (1991) 5883–5890.
- [45] Y. Luo, H. Agren, O. Vahtras, P. Jorgensen, V. Spirko, H. Hettema, *J. Chem. Phys.* 98 (1993) 7159–7164.
- [46] S.P. Neshyba, R.R. Gamache, *J. Quant. Spectrosc. Radiat. Transfer* 50 (1993) 443–453.
- [47] J.O. Hirschfelder, C.F. Curtiss, R.B. Bird, *Molecular Theory of Gases and Liquids*, Wiley, New York, 1964.
- [48] R.J. Good, C.J. Hope, *J. Chem. Phys.* 55 (1971) 111–116.
- [49] R.A. Sack, *J. Math. Phys.* 5 (1964) 260–268.
- [50] B. Labani, J. Bonamy, D. Robert, J.-M. Hartmann, J. Taine, *J. Chem. Phys.* 84 (1986) 4256–4267.
- [51] J.K.G. Watson, *J. Chem. Phys.* 46 (1967) 1935–1949.
- [52] F. Matsushima, H. Odashima, T. Iwaskai, S. Tsunekawa, *J. Mol. Struct.* 352–353 (1995) 371–378.
- [53] J.-M. Flaud, C. Camy-Peyret, Watson Hamiltonian constants for low lying vibrational states of H₂O, Private communication, 2005.
- [54] L.S. Rothman, R.L. Hawkins, R.B. Wattson, R.R. Gamache, *J. Quant. Spectrosc. Radiat. Transfer* 48 (1992) 537–566.
- [55] W.H. Flygare, R.C. Benson, *Mol. Phys.* 20 (1971) 225–250.
- [56] C.G. Gray, K.E. Gubbins, *Theory of Molecular Fluids*, Clarendon Press, Oxford, 1984.
- [57] C. Graham, J. Pierrus, R.E. Raab, *Mol. Phys.* 67 (1989) 939–955.
- [58] D.R. Lide (Ed.), *CRC Handbook of Physics and Chemistry*, 83rd ed., The Chemical Rubber Company, Cleveland, OH, 2003.
- [59] M.P. Bogaard, B.J. Orr, *MPT International Review of Science, Physical Chemistry, Series Two*, in: A.D. Buckingham (Ed.), *Molecular Structure and Properties*, vol. 2, Butterworth, London, 1975, Chapter 5.
- [60] Y. Tanaka, A.S. Jursa, F.J. LeBlanc, *J. Chem. Phys.* 32 (1960) 1199–1205.
- [61] M. Diaz Pena, C. Pando, J.A.R. Renuncio, *J. Chem. Phys.* 76 (1982) 325–332.
- [62] M. Diaz Pena, C. Pando, J.A.R. Renuncio, *J. Chem. Phys.* 76 (1982) 333–339.
- [63] J.-P. Bouanich, *J. Quant. Spectrosc. Radiat. Transfer* 47 (1992) 243–250.
- [64] R.R. Gamache, J.-M. Hartmann, *J. Quant. Spectrosc. Radiat. Transfer* 83 (2004) 119–147.
- [65] A.S. Pine, J.P. Looney, *J. Mol. Spectrosc.* 122 (1987) 41–55.
- [66] L.R. Brown, C. Plymate, *J. Quant. Spectrosc. Radiat. Transfer* 56 (1996) 263–282.
- [67] G. Wagner, M. Birk, R.R. Gamache, J.-M. Hartmann, *J. Quant. Spectrosc. Radiat. Transfer* 92 (2005) 211–230.
- [68] R.A. Toth, L.R. Brown, M.A.H. Smith, V.M. Devi, D.C. Benner, M. Dulick, *J. Quant. Spectrosc. Radiat. Transfer* 101 (2006) 339–366.
- [69] B.K. Antony, S. Neshyba, R.R. Gamache, *J. Quant. Spectrosc. Radiat. Transfer* 105 (2007) 148–163.
- [70] J.M. Hartmann, J. Taine, J. Bonamy, B. Labani, D. Robert, *J. Chem. Phys.* 86 (1987) 144–156.
- [71] G. Birnbaum, *Advances in Chem. Phys.* 12 (1967) 487–548.
- [72] R.R. Gamache, J.-M. Hartmann, *Can. J. Chem.* 82 (2004) 1013–1027.
- [73] M.F. Merienne, A. Jenouvrier, C. Hermans, A.C. Vandaele, M. Carleer, C. Clerbaux, P.F. Coheur, R. Colin, S. Fally, M. Bach, *J. Quant. Spectrosc. Radiat. Transfer* 82 (2003) 99–117.
- [74] P.F. Coheur, S. Fally, M. Carleer, C. Clerbaux, R. Colin, A. Jenouvrier, M.F. Merienne, C. Hermans, A.C. Vandaele, *J. Quant. Spectrosc. Radiat. Transfer* 74 (2002) 493–510.
- [75] D. Jacquemart, R.R. Gamache, L.S. Rothman, *J. Quant. Spectrosc. Radiat. Transfer* 96 (2005) 205–239.
- [76] B.E. Grossmann, E.V. Browell, *J. Mol. Spectrosc.* 138 (1989) 562–595.
- [77] L.R. Brown, R.A. Toth, M. Dulick, *J. Mol. Spectrosc.* 212 (2002) 57–82.
- [78] D. Crisp, D.A. Allen, D.H. Grinspoon, J.B. Pollack, *Science* 253 (1991) 1263–1266.
- [79] J.B. Pollack, J.B. Dalton, D. Grinspoon, R.B. Wattson, R. Freedman, D. Crisp, D.A. Allen, B. Bezard, C. DeBergh, L.P. Giver, Q. Ma, R. Tipping, *Icarus* 103 (1993) 1–41.
- [80] R.R. Gamache, *J. Mol. Spectrosc.* 229 (2005) 9–18.